CHALMERS

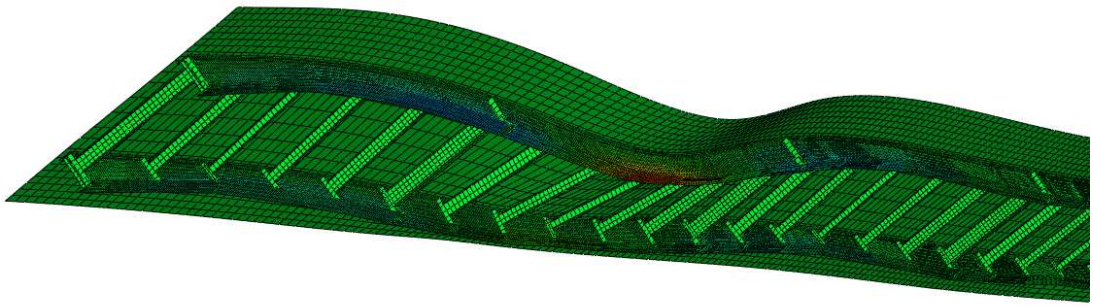

FE-analysis of Vårby Bridge

Investigation of fatigue damage in a composite bridge

Master of Science Thesis in the Master's Programme Structural Engineering and Building Performance Design

ROBERT BENGTSSON
MIKAEL WIDÉN

Department of Civil and Environmental Engineering
Division of Structural Engineering
Steel and Timber Structures
CHALMERS UNIVERSITY OF TECHNOLOGY
Göteborg, Sweden 2010
Master's Thesis 2010:85

MASTER'S THESIS 2010:85

FE-analysis of Vårby Bridge

Investigation of fatigue damage in a composite bridge

Master of Science Thesis in the Master's Programme Structural Engineering and Building Performance Design

ROBERT BENGTSSON

MIKAEL WIDÉN

Department of Civil and Environmental Engineering
Division of Structural Engineering
Steel and Timber Structures
CHALMERS UNIVERSITY OF TECHNOLOGY
Göteborg, Sweden 2010

FE-analysis of Vårby Bridge
Investigation of fatigue damage in a composite bridge

Master of Science Thesis in the Master's Programme Structural Engineering and Building Performance Design

ROBERT BENGTSSON

MIKAEL WIDÉN

Examensarbete / Institutionen för bygg- och miljöteknik,
Chalmers tekniska högskola 2010:85

Department of Civil and Environmental Engineering
Division of Structural Engineering
Steel and Timber Structures
Chalmers University of Technology
SE-412 96 Göteborg
Sweden
Telephone: + 46 (0)31-772 1000

Cover: Moving load in right traffic lane
Chalmers Reproservice / Department of Civil and Environmental Engineering
Göteborg, Sweden 2010

FE-analysis of Vårby Bridge
Investigation of fatigue damage in a composite bridge

Master of Science Thesis in the Master's Programme Structural Engineering and Building Performance Design

ROBERT BENGTSSON
MIKAEL WIDÉN
Department of Civil and Environmental Engineering
Division of Structural Engineering
Steel and Timber Structures
Chalmers University of Technology

ABSTRACT

Vårby Bridge was built in Stockholm in 1996 and serves as a highway bridge. The bridge consists of two adjacent composite bridges with three lanes of traffic each. During inspection of the bridge in the summer of 2006, only ten years after the bridge was opened for traffic, fatigue cracks were observed in several welded connections between the vertical web stiffeners and the upper flange of the main girders. Common for all detected cracks is that they occur only where there is a single vertical stiffener, i.e. not over support.

The purpose of this master thesis was to investigate the mechanisms behind crack initiation, why the fatigue cracks only appear at spans and if cracking is deformation or load induced.

The bridge was modelled with shell elements for the entire bridge, including the concrete deck in the FEM software program Abaqus. First a global model was created and used to verify the accuracy of the model by comparing the bending stresses at certain locations in the main girders with the corresponding values from the on-site strain measurements. In addition to this comparison, a parameter study was performed, including load locations and stiffness.

To capture the stress gradients in the vertical web stiffener of interest, a refined model was created by modifying the global model with a finer mesh in this area and by modelling the applied truck load in a more detailed way.

In the literature study a number of possible mechanisms were found that might induce fatigue cracks in the welded joints studied. A theory why cracks have been found in Vårby Bridge and why only in span is presented. The result of the theory presented argues that cracks are formed by load applied directly above the vertical web stiffeners together with residual stresses causing fatigue cracks.

Keywords: composite bridge, fatigue cracks, vertical web stiffener, Abaqus, FEM, global model, refined model

FE-analys av Vårbybron

Undersökning av utmattningsskador i en samverkansbro

Examensarbete inom Structural Engineering and Building Performance Design

ROBERT BENGTSSON
MIKAEL WIDÉN
Institutionen för bygg- och miljöteknik
Avdelningen för Konstruktionsteknik
Stål- och träbyggnad
Chalmers tekniska högskola

SAMMANFATTNING

Bron som leder E4-an över Vårby-fjärden färdigställdes under 1996 och består av två nästan identiska samverkansbroar, en för vardera trafikriktning. Under en visuell inspektion av bron sommaren 2006 hittades utmattningssprickor i flertalet svetsar mellan vertikala livavstyvningar och överfläns på huvudbalkarna. Sprickorna hittades i fältsnitt men inte i stödsnitt.

Målet med examensarbetet var att tillsammans med Ramböll Luleå undersöka varför utmattningssprickorna i Vårbybron endast uppstår i fältsnitt. För att lösa detta gjordes FE-analyser i programvaran Abaqus som jämfördes med töjningsmätningar utförda på Vårbybron.

Först gjordes en global modell för att jämföra och verifiera böjstyvheten hos bron. Detta gjordes med en grov elementindelning och simulering av fordon med hjälp av punktlaster. Resultatet visade god överensstämmelse mellan uppmätta värden och värden från Abaqus.

Därefter förfinades modellen med avseende på elementindelning och laster för att erhålla bättre spänningsfördelning i området kring svetsarna som studerades. Jämförelsen mellan töjningsmätningar och värden från modellen visade ingen god överensstämmelse på grund av att samverkan mellan betong och stål i bron inte var korrekt modellerat.

Resultat kunde ändå användas för att presentera en teori om varför sprickorna har uppkommit och varför de bara finns i fältsnitt. Trafiklast placerad över en huvudbalk leder till stora tryckspänningar vilket tillsammans med egenspänningar i svetsarna gör att spänningsintervallet för en lastcykel kan vara upphovet till sprickorna. I litteraturstudien presenteras även andra tänkbara teorier för uppkomst av sprickor vilka kan utgöra en förhöjning av spänningsnivåerna när olika lastfall inträffar samtidigt.

Nyckelord: samverkansbro, utmattning, sprickor, vertikal livavstyvning, Abaqus, FEM

TABLE OF CONTENTS

PREFACE

This master thesis was carried out between December 2009 and June 2010 at the Division of Structural Engineering at Chalmers University of Technology together with Ramböll Luleå.

We would like to thank all people involved in this project especially Mattias Nilsson, supervisor at Ramböll, and Mohammad Al-Emrani, supervisor and examiner at Chalmers.

Big thanks to Farshid Zamiri A. and Mustafa Aygül for valuable input and help along the way.

Our roommates at the department, Nikolaus Ljungström and Olof Karlberg, also deserve thanks for keeping a good and joyful working climate.

Göteborg October 2010

Robert Bengtsson & Mikael Widén

1 Introduction

1.1 Background

Vårby Bridge was built in Stockholm in 1996 and serves as a highway bridge. The bridge consists of two adjacent composite bridges with three lanes of traffic each. During inspection of the bridge in the summer of 2006, only ten years after opened for traffic, fatigue cracks were observed in several welded connections between the vertical web stiffeners and the upper flange of the main girders. In common for all detected cracks is that they occur only where there is a single vertical stiffener, i.e. not over support.

The Swedish road authority gave Ramböll AB the task to investigate why the detected cracks have occurred and which measures need to be taken – if any – to prevent possible further propagation of the cracks and ensure integrity of the structural system of the bridge. This master thesis is a part of the investigation conducted by Ramböll, and part of the European project "Brifag" in which Ramböll and Chalmers are involved, why the fatigue cracks occur in the bridge and to find possible ways of retrofitting if necessary.

1.2 Aim and objectives

The aim of the master thesis is to investigate the reasons for the formation of the fatigue cracks found in the Vårby Bridge and the specific objectives are:

- To find possible stress concentrations and what effect(s) that generate fatigue damage in the bridge
- To investigate why cracks only occur in span and not over the supports
- To find suitable retrofitting methods if necessary

1.3 Limitations

This master thesis will only investigate why fatigue cracks occur in the connection between vertical web stiffeners and upper flanges of the main girders. Retrofitting method of the studied welded joints will be examined if the cause of damage is established.

1.4 Methodology

To reach the stated objectives the following methodologies are used:

- A literature study of similar bridges that suffer from comparable fatigue damage
- A numerical analysis of the bridge by creating FE-models in the software Abaqus/CAE 6.8-2

2 Literature study

2.1 Studied reports

In the study focus has been to gather relevant findings from literature available. Interesting information for this thesis is why fatigue cracks occur in the welded area, results from experimental tests, how FE-modelling has been performed and how to retrofit cracks. Only three reports of interest were found and the main reasons are little investigations have been made of the specific bridge construction and language difficulties.

2.2 Background

One of the reports is from Austria (Greiner & Taras, 2009) and investigates a continuous composite bridge, Figure 2.1, which suffers from fatigue cracks. The bridge is 560 m long with spans varying between 70-84 m. In the report a comparison by numerical analysis was made with a second bridge from Austria with structural conditions that were similar to the main object. Also retrofitting methods are tested and evaluated.

Figure 2.1: Studied bridge by Greiner & Taras, 2009

The second report (Sakano, Kawakami, Sakai, & Matsushita, 2007) states that one of the most common fatigue damages in orthotropic steel deck bridges in Japan is cracking in the weld between the deck and the vertical stiffener. The purpose with the report was to evaluate a retrofitting method when cracking has occurred. A fatigue test was done to see the performance of the proposed retrofitting method.

The third report (Okura, Shiozaki, Fukumoto, & Nanjyo, 1995) also has its background in Japanese highway bridges suffering from fatigue cracking at welded vertical stiffeners. Focus in this report lies on how the arrangement of stud shear connectors in a composite bridge influence fatigue cracking in the welded joints between a connection plate and web and top flange.

2.3 Damage and cause

The damages found in the Austrian bridge are both root and toe cracks in the welded joint between vertical stiffener and the upper flange of the main girders, see Figure

2.2. Cracks are found in about 70 % of all these joints. The main causes for the fatigue cracks are change in the bridge construction due to more traffic and that fatigue was not considered in code regulations at the time of design for the bridge.

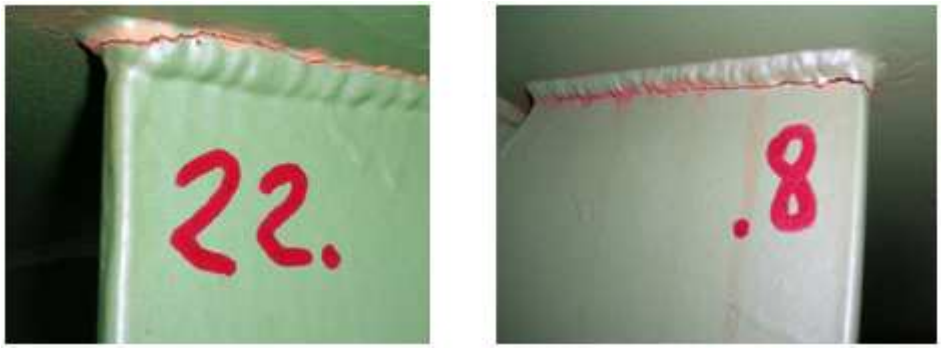

(a) (b)

Figure 2.2: (a) root crack; (b) toe crack, Greiner & Taras (2009)

Originally the deck cantilever was smaller, but due to the more traffic the deck was broadened, Figure 2.3, which lead to a larger cantilever and greater hogging moment. Additionally when the deck was broadened, the deck thickness was decreased to keep the self weight constant.

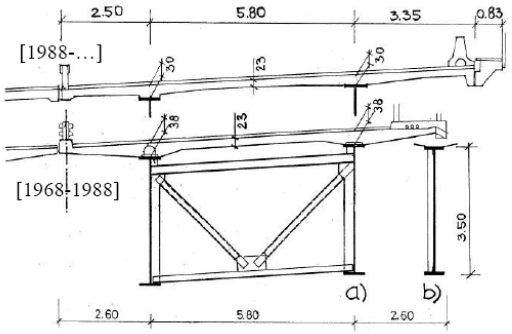

Figure 2.3 Original and broadened deck, Greiner & Taras (2009)

In the report by Sakano et al. (2007) weld toe cracking is considered to initiate when heavy traffic pass over the location of the vertical stiffeners creating severe stress concentrations.

The investigation by Okura et al. (1995) was also regarding the welded joint between vertical stiffeners and the top flange. In Figure 2.4 the different crack types considered in the report can be seen. With consideration to this thesis only one of the types investigated are of interest, type 1 which can be either root or toe crack. No particular cause for damage was mentioned in the report other than the rotation of the slab played a dominant role for type 1 fatigue cracks.

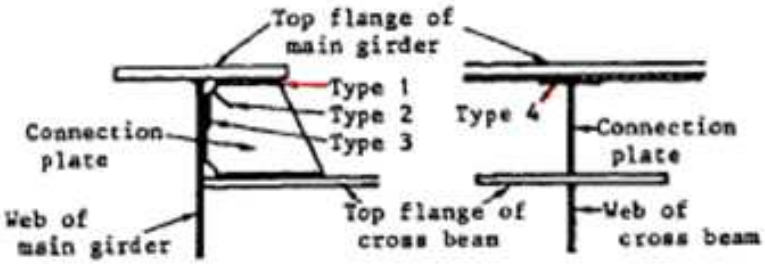

Figure 2.4 Cracks considered by Okura et al.(1995)

2.4 Retrofitting methods

Greiner & Taras (2009) proposed four methods of retrofitting seen in Figure 2.5 and explained below.

a) Replacing fillet welds with full-penetration welds

b) Weld a plate between the flange and the vertical stiffener

c) Make a cut-out at the top of the vertical stiffener

d) Use gusset plates and pre-stressed bolts to be able to remove pre-damaged material close to the cracked welds and place new full-penetration welds in the joint.

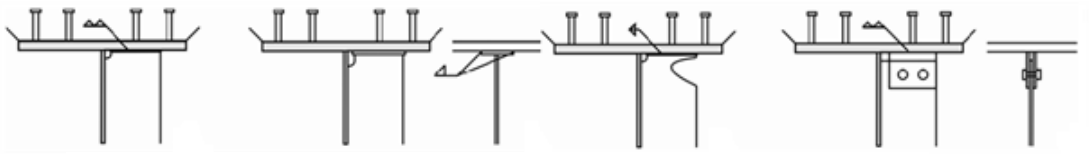

(a) (b) (c) (d)

Figure 2.5: Four methods of retrofitting; (a)-(d), Greiner & Taras (2009)

Method a) increases the fatigue strength in the joint with a factor 2, though it is stated that it is not beneficial to use when repairing cracks in bridge due to the fact that only small portions of the base material can be removed without causing other damage.

Method b) did not work since fatigue cracks developed in the fillet welds connecting the plate to the top flange.

Method c) works in principal, when aiming to transfer the stress maximum to the cut-out in the vertical stiffener and thereby to higher fatigue strength. It is though stated that the geometry of the cut-out should be made in an optimised way and that that is very difficult to obtain when repairing fatigue cracks.

Method d) works though the use of pre-stressed bolts appeared necessary to not cause local stress concentrations due to slip of the plates.

Also Sakano et al. (2007) proposes the use of method c) above and concludes that the stress concentration in the area can be lowered but the propagation of cracks does not stop, though it slows down.

2.5 FE-modelling

In the report by Greiner & Taras, (2009) a comparison was made by numerical analysis between the investigated bridge and another bridge with similar structural conditions. Field measurements were used to verify the model. The results presented stated the magnitude of stresses (tension) at the end of the top edge of vertical stiffener to be between 70-115 MPa in the model and 60-80 MPa from field measurements. The difference was regarded to occur due to difficulties to obtain the correct stiffness in the area. Conclusions in the report stated that the stresses in the model decreases to about 40 % of the value above, when top bracing was not attached to the stiffener and a decrease to 60 % when the studs were out of alignment with the stiffener. The rotation of the concrete slab over the main girder was 0.10° for the investigated bridge and 0.037° for the other bridge. The difference between the bridges was concluded to be the greater slab thickness in the second bridge even though it had a larger cantilever.

A FE-analysis was also performed by Sakano et al. (2007) to evaluate how the stress concentration changes when making a cut-out in the vertical web-stiffener, see Figure 2.6. The result from the analysis stated the magnitude of stresses (compression), before the cut-out, to -961 MPa at the weld-end at the stiffener-side. After the cut-out was made the stress was decreased to -543 MPa and the magnitude of stress in the crown of circle.

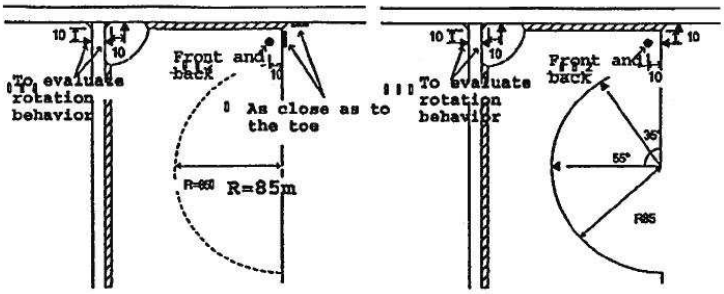

Figure 2.6: Stress concentration, cut out hole in the vertical web stiffener, Sakano et al. (2007)

In the report by Okura et al. (1995) FE-modelling was performed to establish a load-transfer model between the steel deck and the top flange of the girder, Figure 2.7. The connection was modelled using beam elements as stud, with the proper stiffness, and rigid beams with hinges at one side of the flange depending on the rotation of the cross beam and deformation of the deck, Figure 2.8. The load-transfer model was the used to evaluate the influence of stud spacing and arrangement. The conclusions, made by Okura et al. (1995), stated that the spacing and arrangement of studs had no influence when looking on fatigue cracks at the top of the vertical stiffener for this specific case.

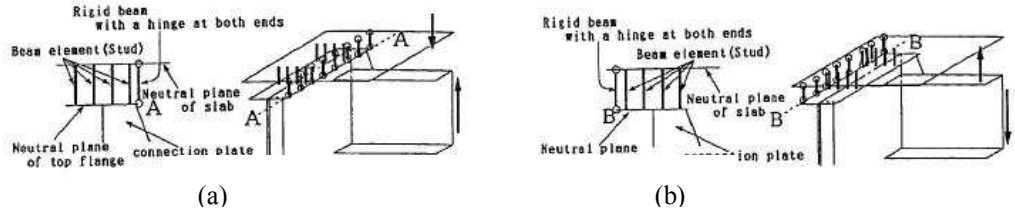

(a) (b)

Figure 2.7: Definitions of rotation and deformation; (a) positive; (b) negative, Okura et al. (1995)

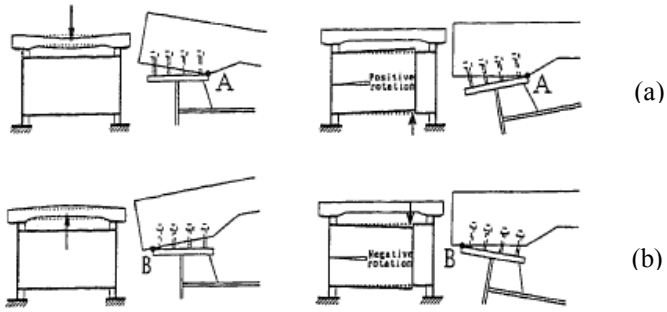

Figure 2.8: Definitions of rotation and deformation; (a) positive (b) negative, Okura et al. (1995)

2.6 Experimental test

The experimental test presented by Sakano et al. (2007), and the only of interest, was a fatigue test with the aim to run until toe cracks were formed at the fillet welds on both deck-side and stiffener-side. When cracks had formed the retrofitting method mentioned above was performed and the fatigue test continued and evaluated to see the effects of the retrofitting. The test was performed on a full-size specimen, Figure 2.9. It is an orthotropic steel deck with trough ribs welded to it and three vertical stiffeners were used, denoted R1-L, R1-R and R2-L

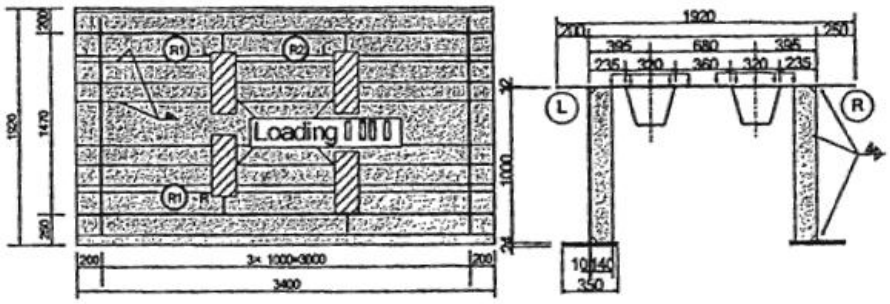

Figure 2.9: The tested specimen by Sakano et al (2007)

After testing was finished it was stated that the crack propagation on the deck side of the fillet weld was stopped, while on the stiffener side propagation continued, though very slow.

2.7 Summary

All the studied reports have the background from bridges suffering fatigue cracks in the main girders at the welded joint between the top flange and the vertical web stiffener.

The cracks found are both weld toe and root cracks.

The causes of initiation of the cracks from the literature are:

- Hogging moment when traffic runs on the cantilever of the deck causing too high tensile stresses in the weld.
- When the traffic load is applied over the vertical stiffener causing high compressive stresses in the top edge of the vertical stiffener together with tensile residual stresses in the welds.

Two causes for crack initiation were found during the literature study. This might not be the effects causing fatigue cracking in the bridge investigated in this thesis. Therefore a few additionally possible causes are stated below:

- When traffic load is applied in the centre of the deck transversally, causing rotation of the deck which generates high compressive stresses together with tensile residual stresses in the welds.
- Another cause of cracking when traffic load is applied on the main girders, apart from the one above, is the influence of the rotational rigidity of the cross section. If the rigidity is too small the displacement of the main girders will be uneven i.e. the loaded girder will rotate around the other girder causing compressive stresses in the weld at the stiffener on the unloaded girder. Together with tensile residual stresses this can cause cracking. In addition to compressive stresses also shear stresses can occur in the weld due to the influence of cross beams attached. This behaviour will though not be at the support since the rotation is prevented.

The FE-analysis performed can be summarised with the conclusion that it is difficult to model the stiffness of the cross section in a correct way and that the results tend to be higher in the model than from field measurements.

Regarding retrofitting method a cut-out in the stiffener would work to lower the magnitude of the stress concentration according to Sakano et al. (2007), though Greiner & Taras, (2009) suggests it is difficult in practice due to the cut-out needs to be made with geometrically good precision and therefore difficult and time consuming to apply on a bridge. Further Greiner & Taras, (2009) proposes two methods that work both in theory and for use in practice.

Additionally a thought about the necessity to apply retrofitting methods is if the fatigue cracking is load or deformation induced. The methods above is to prevent load induced cracks, if deformation induced cracks are formed it will perhaps be enough to make control measurement of the cracks in certain intervals to ensure that they does not propagate further.

3 Vårby Bridge

3.1 Description

In the summer of 2006 an inspection of the bridge was made and several fatigue cracks were found. To find the origin of the cracks Ramböll AB was given the task to investigate the bridge. As a part of the investigation strain measurements were performed on the bridge (James & Kärrfelt, 2009). Below the bridge dimensions are presented followed by a description of the damage found and also how the measurements were carried out.

Since the bridge consists of two adjacent composite bridges only one of these will be described below. The bridge chosen is the one called the "North Bridge", because the strain measurements were performed there.

3.2 Dimensions and general features

The bridge is a continuous bridge with six spans over seven supports. The four inner spans are of equal length, 44m, and the end spans are about 38 m long, Figure 3.1. The main girders in the spans are of varying height, where the height is at maximum over the support and minimum at mid-span. Between support and mid-span the girder height varies linearly, naturally with the top of the girder kept horizontal.

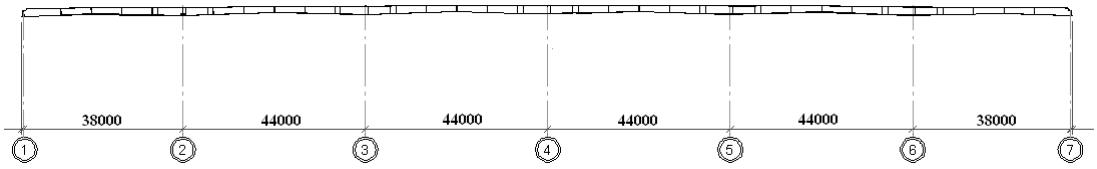

Figure 3.1: Elevation of the six spans in Vårby Bridge. (1) and (7) corresponds to end supports and (2) – (6) mid-supports.

The composite bridge consists of steel I-girders and a concrete deck. Between the main girders there are cross-beams in the shape of I-beams working as diaphragms. The functions of the cross-beams were both during the casting of the deck and when the bridge was finished. During casting they were used to prevent lateral buckling of top flanges in compression and when the bridge was finished to provide resistance against lateral forces and to distribute hogging bending moment from main girders. The cross-beams are attached to the vertical web-stiffeners by bolts through the vertical web stiffeners, Figure 3.2. Although the girder heights vary, the distance between the top flanges in the main girders and the top of the cross-beams remains constant to 400 mm which can be seen in Figure 3.3.

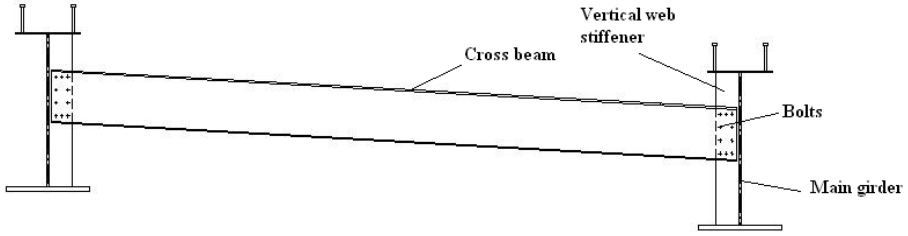

Figure 3.2: Diaphragm in span where the two main girders are connected by a cross-beam through bolts. The two main girders are displaced in vertical direction due to the road building of the highway

In total, there are 28 cross-beams in the 6 spans and also one cross-beam over each support. Three different cross section types are used all over the bridge at the positions of the vertical stiffeners in the spans. Over the intermediate supports one cross section type is used and also one type for the two end supports.

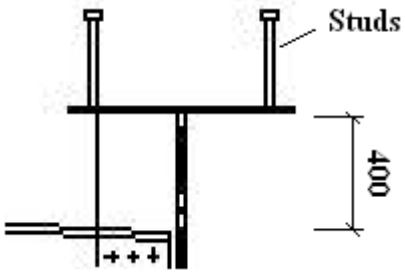

Figure 3.3: A constant distance of 400 mm between the top flange and cross beam for all diaphragms in Vårby Bridge

There is one difference between the cross sections for the spans compared to the supports, over the supports there are double vertical web stiffeners and in the spans there is a single stiffener. Figure 3.4 show a diaphragm at support with two vertical web stiffeners. The geometry of the different types of cross sections and the remaining dimensions for the two main girders etc, are presented in Appendix A.

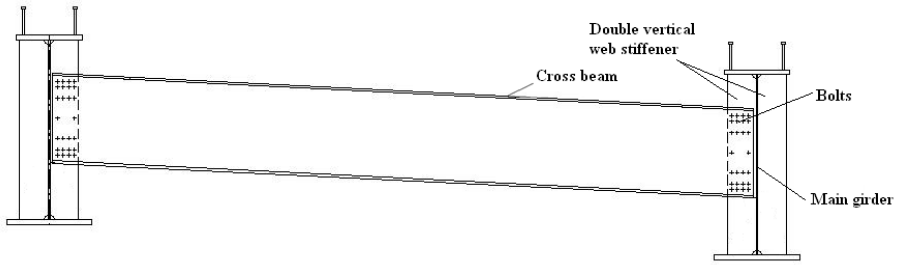

Figure 3.4: Diaphragm at support with double vertical web stiffener

The concrete deck has a free width of 14000 mm. The deck varies in thickness between 350 mm, which is at the area connected to the top flanges of the main

girders, 170 mm which are at the end in the close proximity to the end beams and 280 mm along the centre line of the bridge.

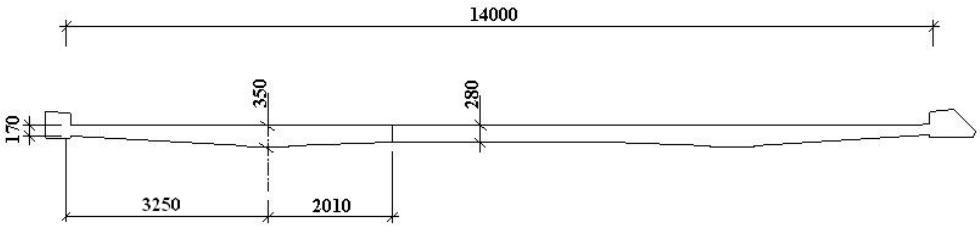

Figure 3.5: The concrete deck with dimensions

To receive the composite action between the concrete deck and the main girders studs are used in Vårby Bridge visible in figure 3.3. The studs are placed in two rows along the bridge with spacing of 550 mm in transversal direction and in longitudinal direction the spacing varies between 150, 190 and 260 mm.

3.3 Damage

During the visual inspection in 2006 cracks were found at several welded connections between the vertical web stiffeners and main girder top flange, see Figure 3.6. The cracks found were weld toe cracks, see Figure 3.7, caused by fatigue.

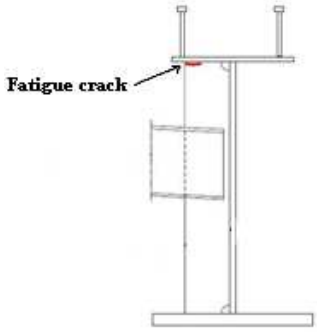

Figure 3.6: Location of fatigue cracks, James & Kärrfelt, (2009)

Figure 3.7: Toe crack at a vertical web stiffener, James & Kärrfelt, (2009)

The damages were observed all over the bridge without any particular pattern, Figure 3.8. One thing though when observing the location of the cracks is important, there are no cracks found in the connections at the supports.

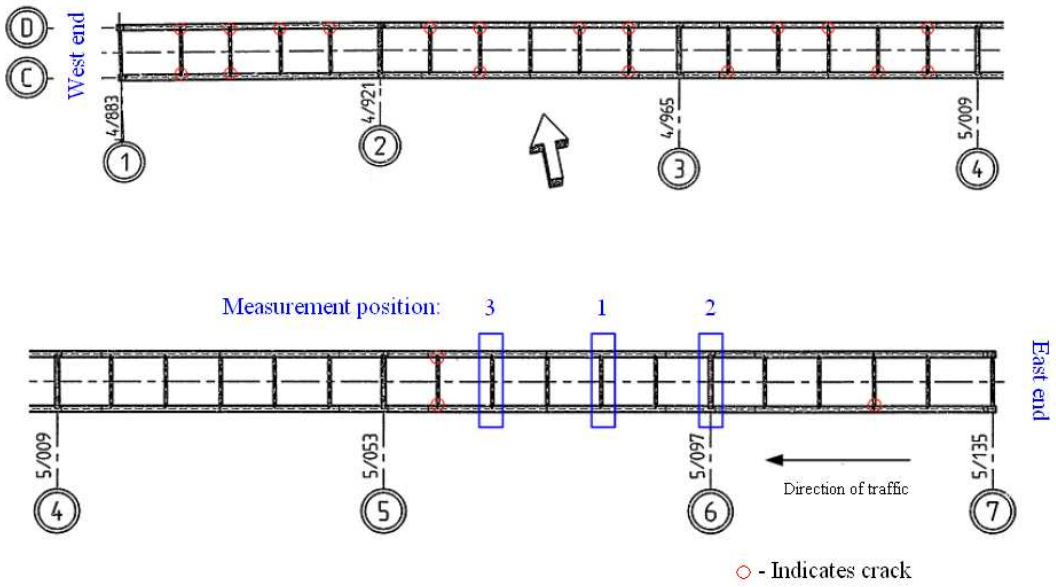

Figure 3.8: Fatigue cracks observed at the visual inspection 2006, James & Kärrfelt, (2009)

In May 2009 a more thorough inspection of one span was made which lead to an increase in cracks found. Previously 2 cracks were noticed but the new investigation found 7, including the old ones, see Figure 3.9. Also the total lengths of the cracks were measured and the magnitude lies in the range of 15-30 mm. The inspection was made because the measurements were later performed in this span. No more inspection has been made on the bridge to the awareness of the authors of this thesis though the additionally found cracks in the more investigated span indicates that there are more cracks than shown in Figure 3.9

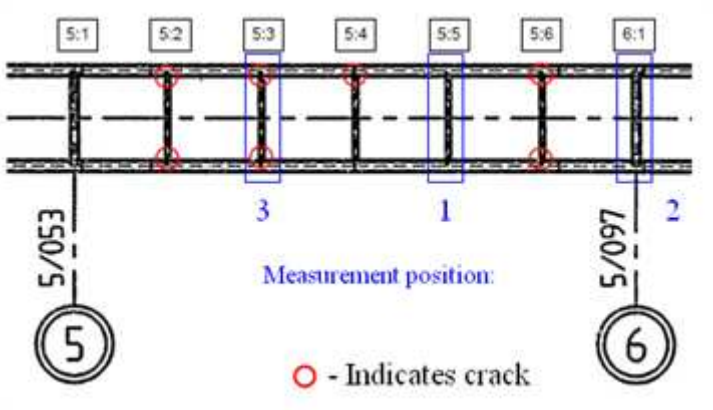

Figure 3.9: Fatigue cracks observed in the inspection 2009 in the span between support 5 and 6 where the strain measurements are performed, James & Kärrfelt, (2009)

To investigate the initiation and propagation one sample was deducted from a crack.

The conclusions drawn by Eriksson, (2009) were:

- No particular defects of the weld was found
- No defects found in the heat affected zone (HAZ)
- Multiple initiations, which means that two separate cracks initiated independently of each other. This behaviour should appear after a large amount of cycles.
- The cracks propagated and were merged together.
- The origin of initiation cannot be fully concluded due to severe corroded crack surfaces.
- The corrosion decreases with depth of the cracks
- The propagation was determined to be disturbingly rapid with typical beach marks and striations. The speed of the propagation was due to the fact that two cracks were closing in on each other, leaving smaller and smaller thickness of the base material.
- It was concluded that the cracks was a result of fatigue.

3.4 Measurements

The strain measurements performed on the bridge were made in June 2009 by James & Kärrfelt, (2009) and consisted of three different types of measurements:

- The first measurement was done when the equipment were placed on the bridge. The outcome from this occasion was to be used to evaluate if the position of the points of measurements were satisfying or needed correction. Below the positions chosen and the locations of the equipment are presented.
- The second type of measurements was done when loading the bridge with a truck of known weight. The idea behind this was to use the result when calibrating a FEM-model of the bridge.
- A free flow measurement was also done during approximately 5 days to evaluate what magnitude of stresses and stress range that could be expected caused by ordinary traffic.

3.4.1 Location of measurement equipment

The measurement equipment was placed at three different diaphragms, position 1, 2 and 3 which can be seen in Figure 3.9 above. Each diaphragm in the bridge is denoted with a letter and a number. Below this notation are used to describe which diaphragm regarded. In Appendix A the notations are stated.

Position 1 is at diaphragm F23 where no cracks in the welded joints of interest were found. The locations of the equipment are presented in Figure 3.10. As can be seen in the figure there are strain gauges applied at the bottom of the main girders to measure the global behaviour of the bridge and to obtain influence lines.

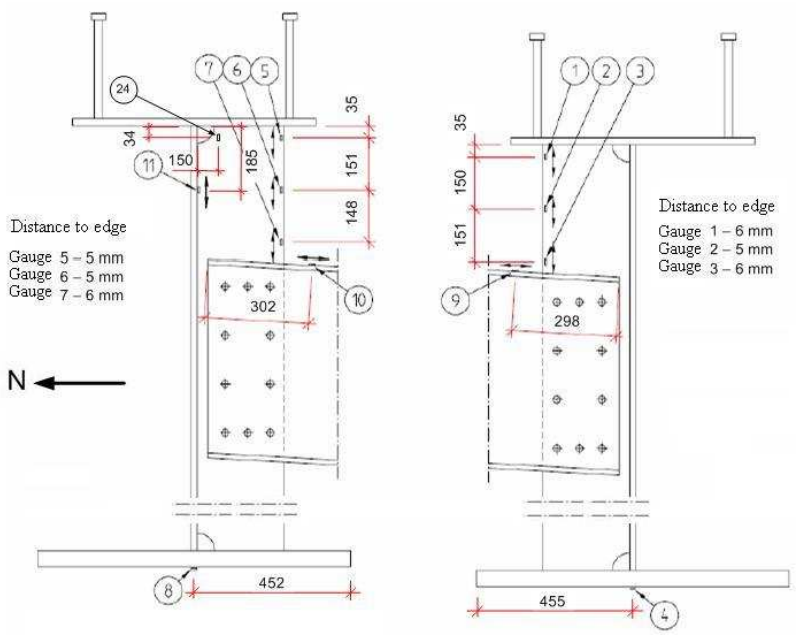

Figure 3.10: Measurement position 1, in span; no cracks observed, James & Kärrfelt, (2009)

Position 2 is over support B6, which is also an cross section without cracks, and chosen to use as comparison with the measurements in position 1 to answer the question why cross sections above support do not suffer from fatigue cracks. The locations of the equipment are seen in Figure 3.11.

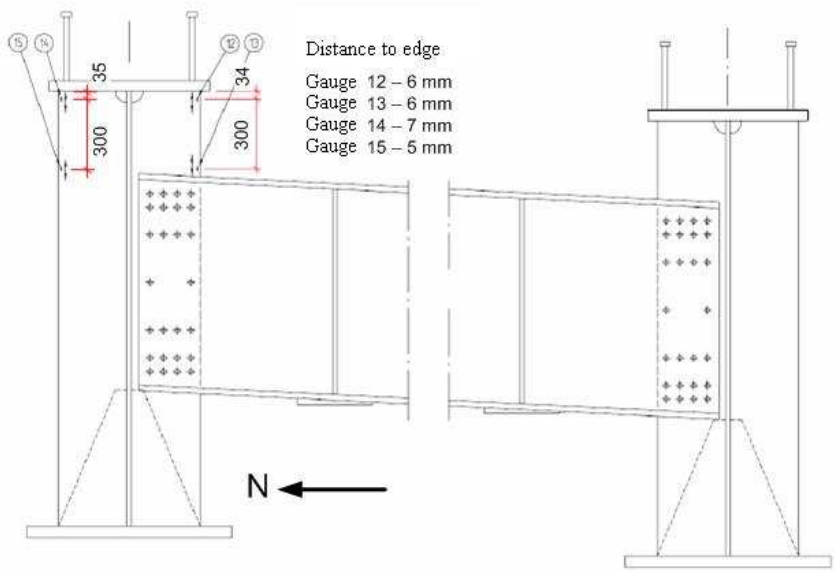

Figure 3.11: Measurement position 2, at support; no cracks observed, James & Kärrfelt, (2009)

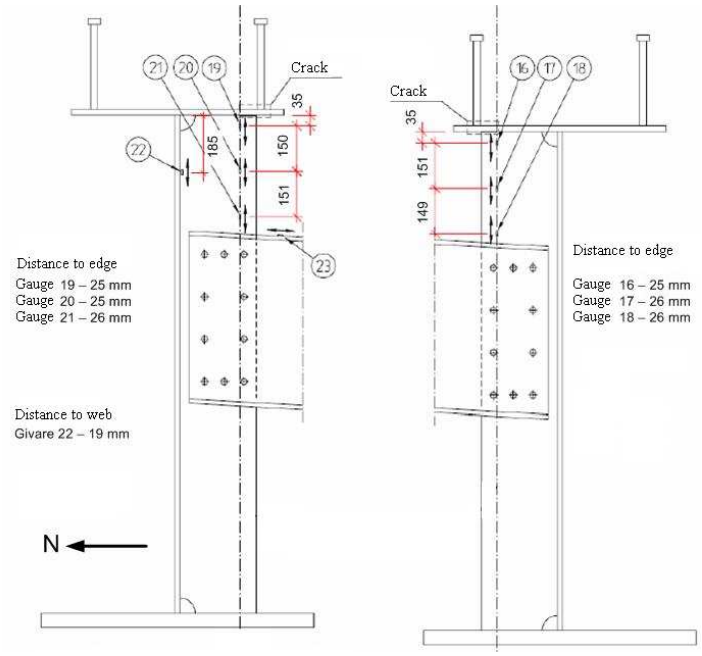

Figure 3.12 Measurement position 3, in span; cracks observed, James & Kärrfelt, (2009)

Position 3 is in the same span as position 1 at diaphragm F21. The cross sections at F21 and F23 are identical geometrically, but F21 suffers from cracks in both welded joints of interest and was therefore chosen. In Figure 3.12 the locations of the equipment are shown.

3.4.2 Strain measurement with known vehicle data

As mentioned above the second type of measurements were made with a truck of known weight and distances between tyres. After loading the truck with stone dust, of 0-8 mm size, the front axle and rear bogie were weighed to 7.38 and 14.26 tonnes respectively. The distances between the tyres are shown in Figure 3.13.

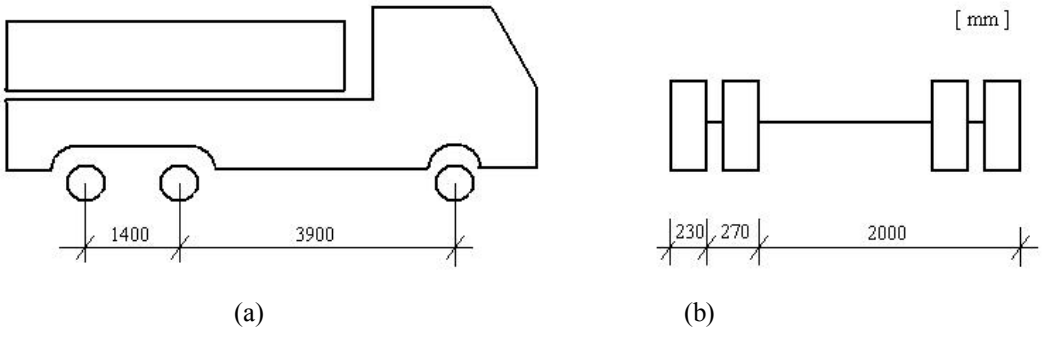

Figure 3.13: Distances between the tyres of the truck with known weight: (a) wheel base, (b) wheel tracks

The measurements were performed during night due to that the bridge was not allowed to be closed down for traffic. As mentioned before, the bridge has three lanes and also a strip of width 2.5 m which is not intended for traffic. The additionally strip

width was measured on site while the width of the ordinary traffic lanes were approximated, see Figure 3.14.

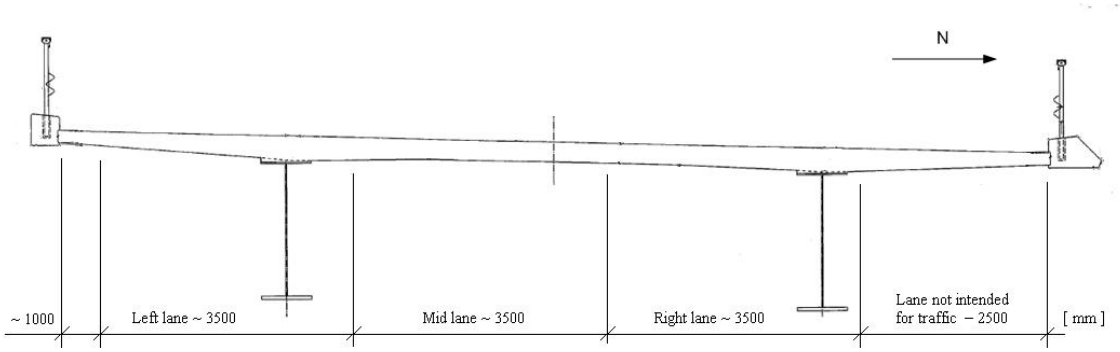

Figure 3.14: Width of each traffic lane, James & Kärrfelt, (2009)

In total 21 different measurements were performed and the difference between them are the location, which lane the truck drove in, and the speed of the truck

Three measurements were chosen, one for each traffic lane with an additional measurement for the lane not intended for traffic (outer lane), to use when verifying the FE-model. This is further presented in chapter 5.

4 Pre-modelling phase

4.1 Pre-modelling phase

In order to be able to model the Vårby Bridge in a proper way and to obtain reliable results, a test were performed in the software Abaqus to evaluate which type of element that should be used when modelling the entire bridge. For this, a number of simple small-scale models with two I-girders and a concrete deck were created. In addition to good results, computational speed and simplicity when constructing the models were taken into consideration. One additional aim with the small-scale models was to find a suitable way to model the composite action between the concrete deck and the I-girders.

For the deck 3-D deformable shell elements were chosen for all models as beam elements are only a line assigned a certain cross-section in Abaqus and is therefore not an option for modelling the deck in the bridge due to difficulties when applying loads on the deck. Solid elements were rejected for both the I-girders and the deck due to the desire of keeping the model small with regard to the computational speed

The two I-girders were decided to be modelled in four different ways with a mixture of 3-D deformable shell and beam elements inspired by Chung & Sotelino (2006) who used these types in their report. Element type B32 is used for the beam elements and QUAD S8R for the shell elements including the deck. The four models are presented in Figure 4.1

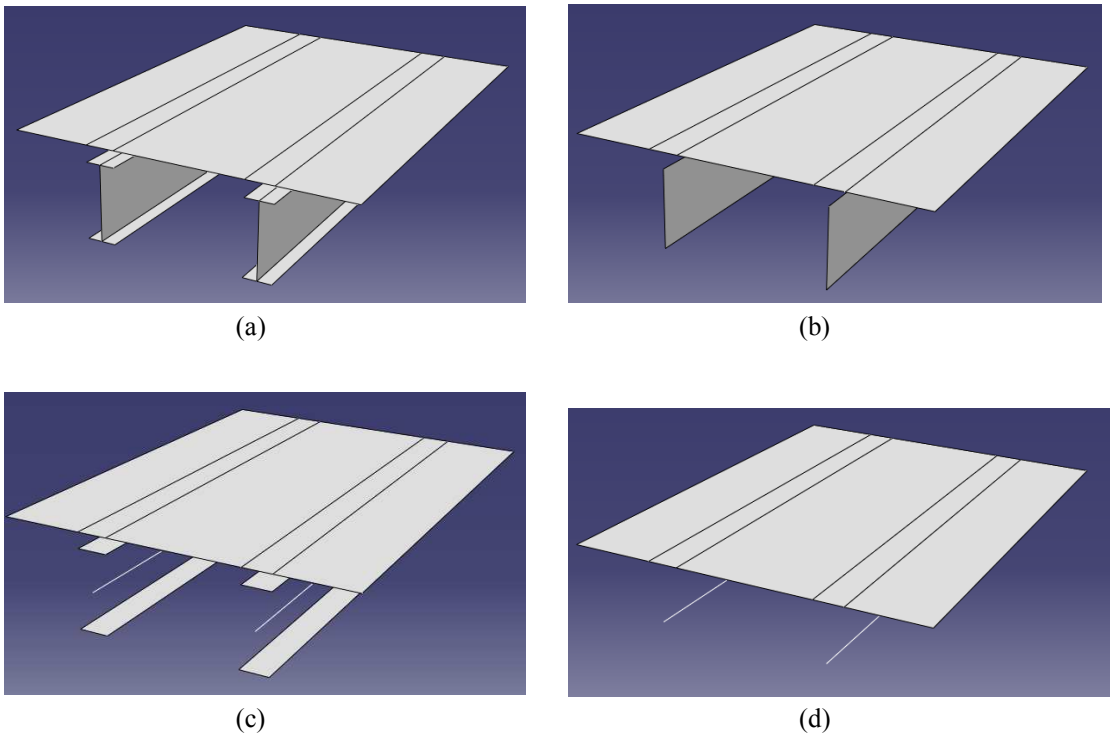

Figure 4.1: The 4 small scale test models (a) shell elements, (b) flanges as beam elements and webs as shell elements, (c) flanges as shell elements and webs as beam elements, (d) beam elements

To get interaction between the upper flanges and the deck in the models a "tie constraint" was used. Using this type of constraint the flanges are, whether they are made of beam or shell elements, fully bonded to the adjacent area in the deck corresponding to the width of the flanges.

During the pre-modelling phase, problems occurred considering how to construct the final bridge model. Since the I-girders in the Vårby Bridge have varying height and flange thickness this should be modelled as well in order to obtain the correct stiffness in the bridge model. In Abaqus it is not possible to construct a beam element with varying cross section, which makes it inappropriate to use. The only way to use beam elements with varying cross section is to divide the element in satisfyingly small parts and assign each part the correct cross section geometry. This is very time consuming and by means of this; both model 3 and 4 were excluded as possible modelling techniques in the bridge model. Model 2 with the webs as shell elements and the flanges as beam elements is possible to use by creating "stringers" at the corresponding edges on the webs. These can be chosen as beam elements and assigned different cross-sections, such as plates. However, there is a need of using offset for the flanges (further explained below) and that is only possible for the stringers using "trapezoidal section" which makes it inconvenient to use for the bridge model. Due to the shortcomings of model 2-4, the fact that the analysis in Abaqus are linear static and that model 1 are easy to construct, model 1 was chosen for the bridge model. Modelling with shell elements also gives a good overview of the geometry when creating the parts and makes it possible to partition the shells in order to attach loads or different thicknesses and it is easy to collect results in the right nodes which are important features in the global analysis.

The shell elements for the flanges were all placed directly on the edge on the web which is not the correct point of gravity centre. To solve this offsets were made to move the flanges (though not physically in Abaqus) to get the true stiffness of the cross section, Figure 4.2.

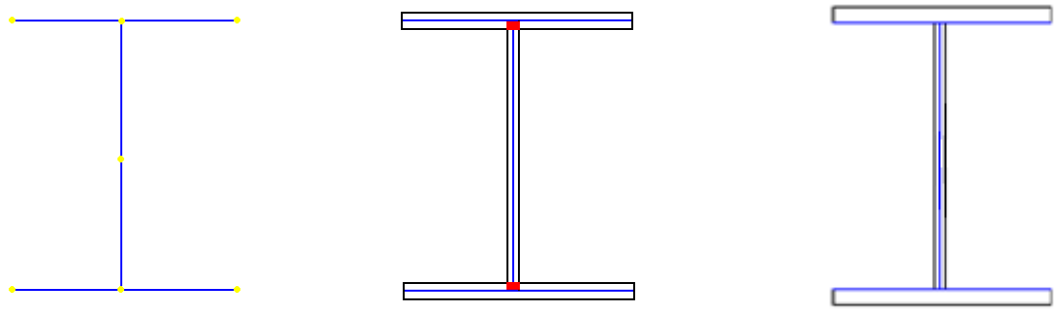

(a) (b) (c)

Figure 4.2: Cross-section of an I-girder with; a) infinite thin shell elements, b) elements assigned a thickness, the red marks show the decreased lever arm of the flanges leading to reduced stiffness for the cross-section, c) flanges attached by using offset giving the correct stiffness

The deck was placed in its gravity centre leading to a gap between the top flanges and the deck in the model which can be seen in Figure 4.3.

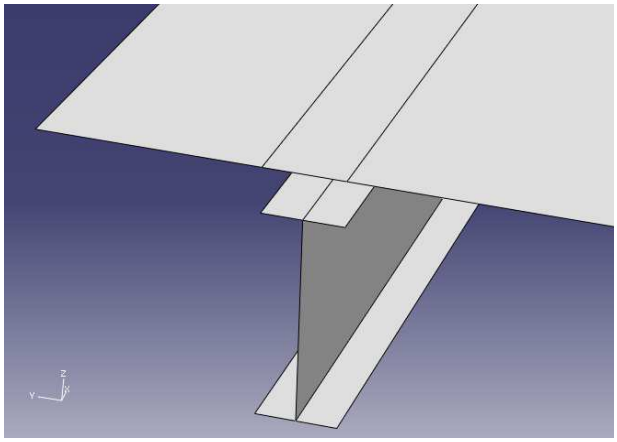

Figure 4.3: The deck distanced by half its thickness plus the thickness of the top flange away from the top flange

The girders were modelled as simply supported and the boundary conditions were placed at the end of each bottom flange in x-direction. To model a simple supported boundary condition one end was free to move in x-direction and rotate around z-axis, while the other end only was allowed to rotate around z-axis. The load used to test the model was of the magnitude of 0.05 MPa and uniformly distributed on the deck in the area over the girders. The mesh varied in size for different parts of the bridge as a consequence of using tie constraints. When using tie constraints in Abaqus the software requests the slave surface to have a finer mesh than the master surface in order to obtain better results and to shorten the run time for the analysis.

To ensure that model 1 function as expected a comparison between deflections obtained from Abaqus and hand calculated ditto were made, see Appendix B. Also the general looks of the loaded model was checked to see that the deformation was reasonable and that the tie constraint between the top flanges and the deck worked satisfyingly.

5 Global FE-analysis

5.1 Introduction

The Vårby Bridge is modelled with 3-D deformable shell elements following the outcomes in the previous chapter. The composite bridge model is build up from 4 different parts for the steel details and one part representing the concrete deck. The analyses performed of the global bridge model are linear static and verified by the on-site strain measurements presented in chapter 3.4.

The materials used in the bridge model are linear elastic with isotropic behaviour, displayed in Table 5.1 below.

Table 5.1: Linear elastic materials used in the bridge model

Material	Density [kg/m^3]	Young's modulus of elasticity[GPa]	Poison´s Ratio
Steel	7850	210	0.3
Concrete	2300	50	0.25

5.2 Steel details

The steel parts were modelled by first sketching the web plate in one of the main girders with regard to the coordinates for the vertical web stiffener, Figure 5.1. These coordinates was used in the following step to extrude the vertical web stiffener and the stiffeners at the support, Figure 5.2.

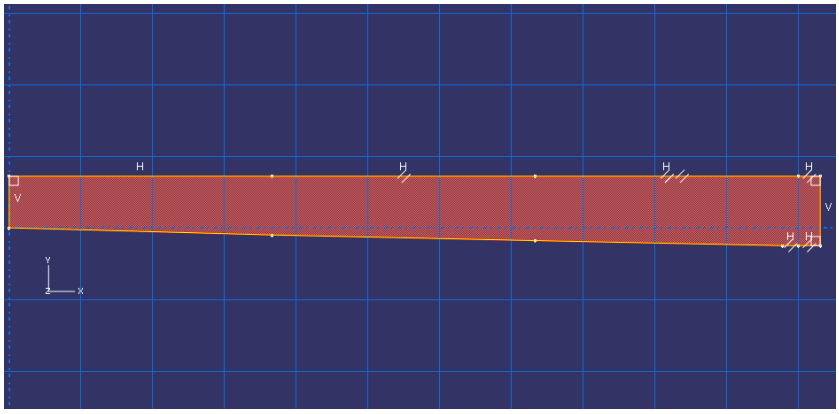

Figure 5.1: The web plate in one of the main girders in sketch mode

The top and bottom flanges were attached to the web plate using offset; the girder was then laterally transposed in order to create the adjacent main girder.

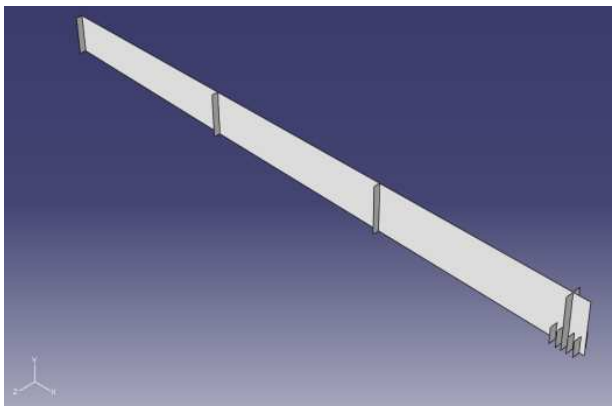

Figure 5.2: The web plate with vertical web stiffeners and stiffeners at support

Cross beams were inserted between the main girders to finalise the part. The described procedure was used to create all the parts for the steel details. Steel parts 1-4 are presented in Figure 5.3.

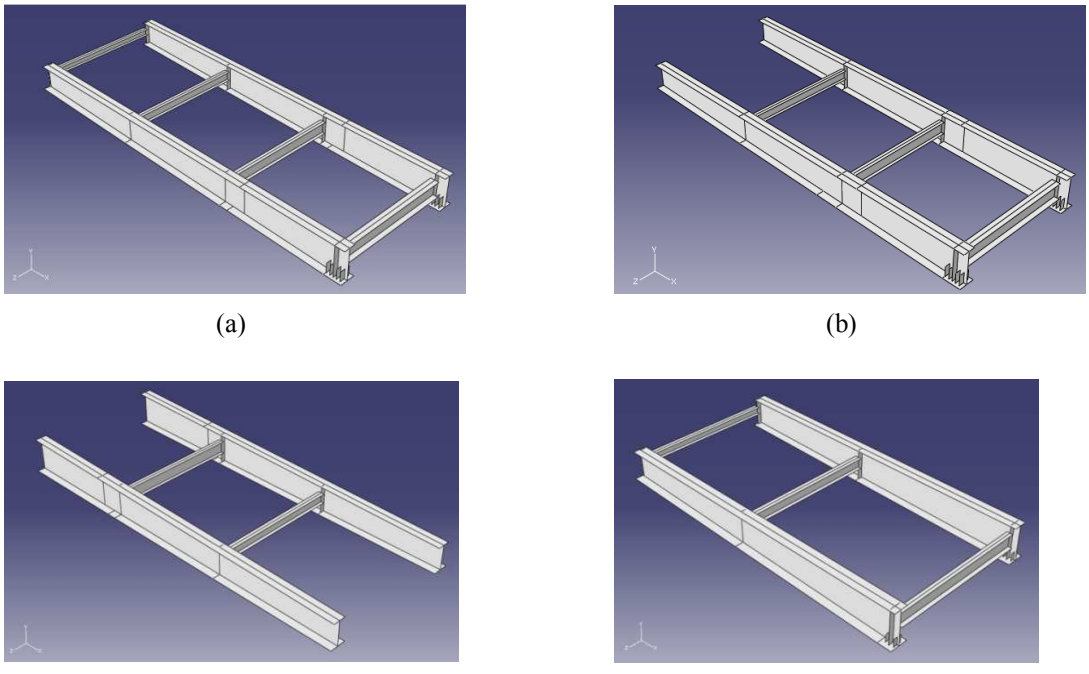

(a) (b)

(c) (d)

Figure 5.3: The steel details in the bridge model: (a) steel 1 (b) steel 2 (c) steel 3 (d) steel 4

Varied compositions of these parts were then assembled together to create the different spans which can be seen in Figure 5.4. The spans assembled together have a total length of 252.6 m.

Part	Steel 1	Steel 2	Steel 3	Steel 4
Colour	Green	Red	White	Blue

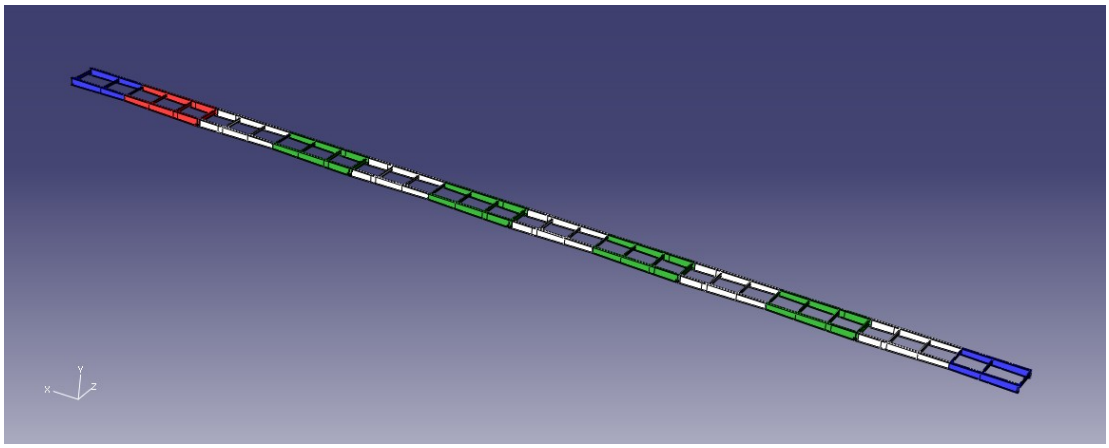

Figure 5.4: The steel parts assembled together in varied composition denoted by different colours for each part

5.3 The deck

The deck is divided into a number of different strips along the bridge in order to simulate the different thicknesses of the concrete deck, Figure 5.5. The composition of the strips is symmetrically arranged around the centre line in longitudinal direction in the deck. The outer most strip is representing the edge beam of the concrete deck and the fourth strip, counting from every long side, have the same width as the top flanges in the main girders due to the connection between the deck and the top flanges.

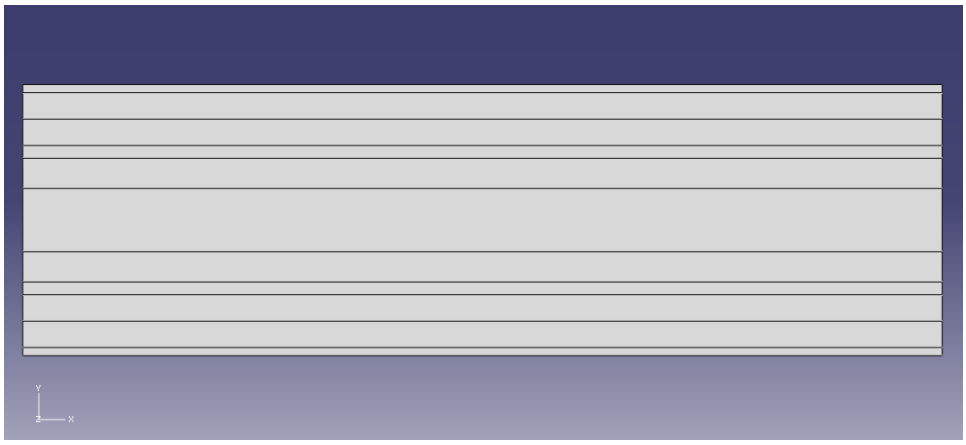

Figure 5.5: The figure shows 1/5 of the bridge deck. The different strips represent varying thicknesses in the deck

Because of the thickness of the deck, (fourth strip), and the thickness of the top flanges, the deck is distanced by 195 mm in order to receive the correct centre of gravity for the co-operating parts. The dimension of the deck is 252.6 m x 14.9 m

5.4 Loads

To be able to verify the global behaviour of the bridge model, a number of load steps were created in order to simulate the moving truck load from the on-site measurements. The loads from the tires, wheel track distance 2010 mm, were represented by 2 point loads for the front tires and 4 point loads for the bogey. The load was applied for each traffic lane in the beginning of the bridge and moved towards the mid-span. The distances between each load step along the bridge varies between 1.0 m and 2.126 m. The shorter distance were used in the interesting area were the largest number of strain gauges (diaphragm F23) is located. Partition lines were sketch with the chosen load step lengths along the bridge. These lines containing 64 nodes (vertices), one for each wheel track.

The vertices were imported into a script-file who distributes the point loads between the vertices for every load step. The bridge models were loaded at a total distance of 139.2 m consisting of 68 load steps. 4 additional steps were created in the beginning and in the end due to that not all of the truck is on the bridge deck at these steps. If a point load is located between two vertices, the script-file distributes the load between these two which can be seen in Figure 5.6 where 4 point loads in the bogey are spread out to 8.

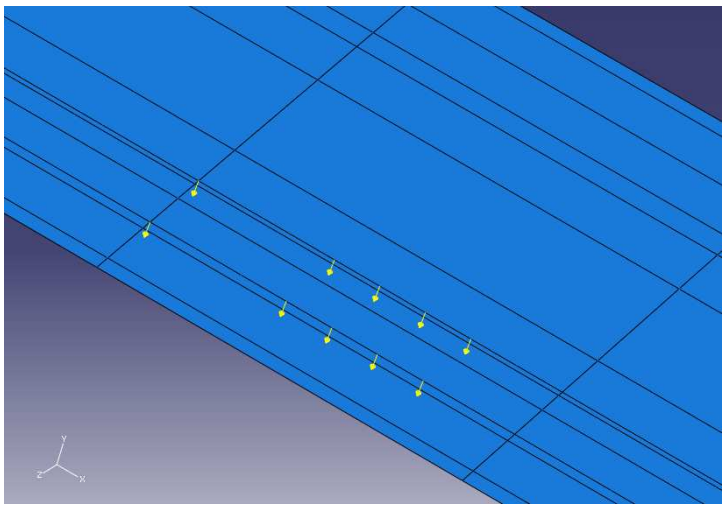

Figure 5.6: Distributed load on the bridge deck representing the moving truck in the on-site measurements

5.5 Boundary conditions

In the Vårby Bridge there are 7 supports which for the two main girders give 14 boundary conditions which can be seen in Figure 5.7. The bridge is free to move in the bridge axis (x-axis) for both main girder C and D, but in transversal direction (z-axis) only for main girder C. This applies for all supports, except in the mid supports where the bearings are fixed for main girder D and partially fixed for main girder C.

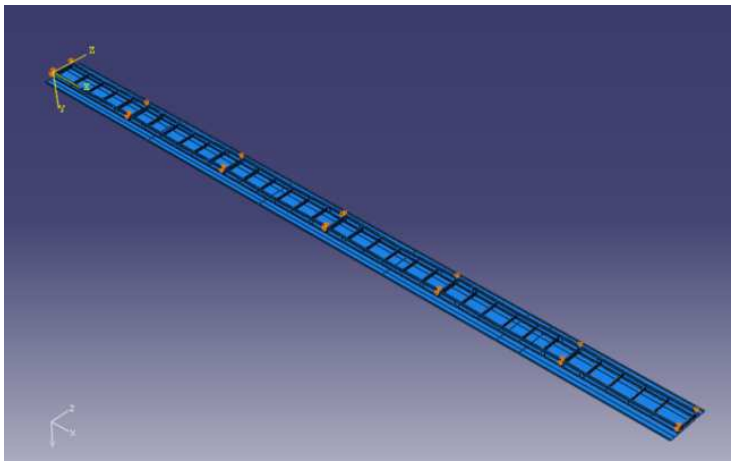

Figure 5.7: Boundary conditions in the bridge model; y-axis represent the vertical direction

The 4 groups of different boundary conditions used in the bridge model are presented in Table 5.2.

Table 5.2: Table over the different boundary conditions for main girder C and D

	-x	-z	-y	Rotations		
C	Free	Free	Fixed	Free	Free	Free
C;mid support	Fixed	Free	Fixed	Free	Free	Free
D	Free	Fixed	Fixed	Free	Free	Free
D; mid support	Fixed	Fixed	Fixed	Free	Free	Free

The boundary conditions are attached to one node located directly under the web in the main girders and in line with the vertical web stiffeners. To represent the bearings in a reasonable way the horizontal plate under the vertical support stiffeners in the bottom flange are free to rotate around the node using a Multi point constraint ("MPC Link"), Figure 5.8.

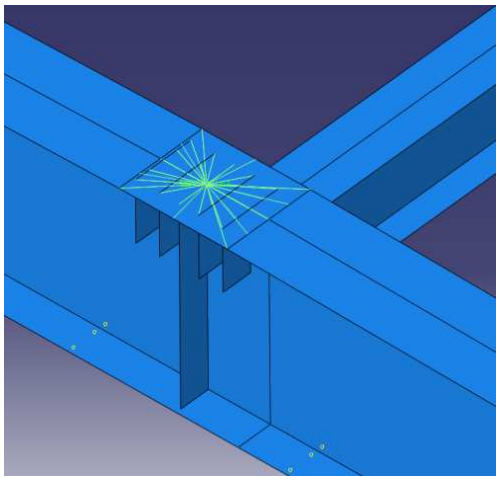

Figure 5.8: Multi point constraint representing the bearings in the supports

5.6 Mesh evaluation

To see that the results are reasonable and capture the expected results in a correct way, a mesh evaluation was performed using a quadratic 8-node doubly curved thick shell element with reduced integration (S8R). The quad-shaped element is used with free technique, medial axis with minimizing the mesh transitions when appropriate. The mesh is seeded by using global seeds for the entire part. To study the differences in the results for different element sizes a range of 200 to 1750 mm was chosen for the steel part in the composite span.

Other parameters that the study investigates are computer usage to run a certain job, smaller elements increase the computer run time, and the difficulty level (time) to achieve a certain mesh. It is preferable if the mesh could be generated in an easy and fast way but still give good results. Table 5.3 summaries the chosen element sizes with related number of elements and run time for a certain job

The study is performed at one of six free spans in the Vårby Bridge. The part of the bridge (in the following denoted as the span) are simply supported with a total length of 45045 mm and with a distance between the supports of 44000 mm. The span is loaded in the middle by a concentrated point load placed at three positions; at the console, over one main girder and at mid strip in transversal direction. The chosen load locations are selected so that different actions of the span can be captured due to the three traffic lanes on the bridge. Two positions are checked with regard to stresses and one of them for deflection; see Appendix C.

Table 5.3: Chosen element sizes in the mesh evaluation with number of elements in vertical direction, number of elements in the span and run time in seconds

Element size	1750	1500	1250	1000	750	600
Web, y-axis	3					
Nr of elements	1127	1272	1417	1584	2006	2366
CPU [s]	24		26			28

Element Size	500	400	300	250	220	200
Web, y-axis	4	5	6	7	8	9
Nr of elements	3115	3999	5580	6905	8442	10361
CPU [s]	32	34	40	49	52	63

The largest element size, 1750 mm, was found to be the maximum value in order to keep the quadratic form. The mesh with the highest number of elements contains 9 elements in y-direction; *s*maller elements than this are not reasonable to use in the global analysis phase. Figure 5.9 show the span without the concrete deck meshed with element size 500 mm. The element size in the concrete deck (size 1000 mm; deck dimension 45045x14900 mm) remains constant for the different element sizes in the steel part.

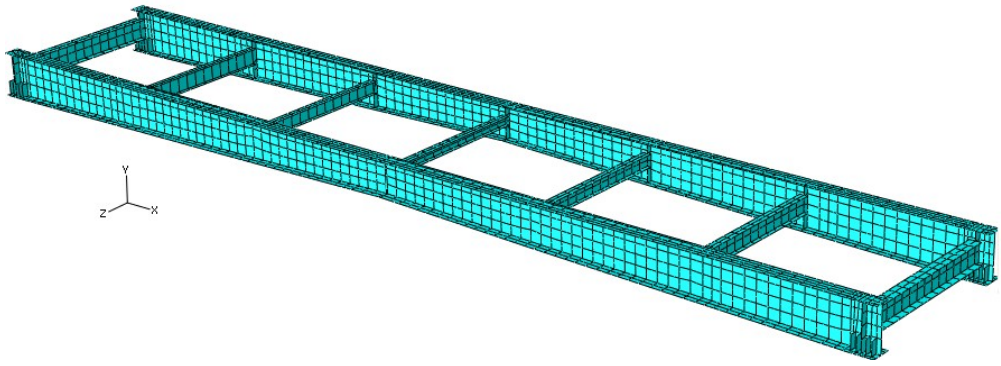

Figure 5.9: The span with 4 elements in the vertical direction, quad-shaped mesh generated by global seeds for the whole part

The evaluation of the different element sizes show that for deflection either one of the different sizes can be used but for the stresses the size must be smaller in order to receive good results, down to 200-300 mm.

The difference in CPU time for the different analysis is negligible and its only takes a few seconds to generate the mesh. Due to this, an element size of 250 mm is a good

choice; especially when the smallest parts (vertical stiffeners) in the bridge model are of 250 mm width, which will enhance the ability for the software to produce a good quality mesh.

5.7 Approximations

5.7.1 Stiffness of the cross section

When modelling with shell elements it is of significant importance that the elements are connected to each other in their respective (end) nodes in order to obtain the correct behaviour. In the Vårby Bridge, the main girders are cambered and the sub parts (web and flanges) vary in thickness along the bridge which also affects the height of the web. The web plates have certain geometry so that the flanges with different thicknesses can be welded to the web plate creating a straight line at the outer surface of the flanges, see Figure 5.10.

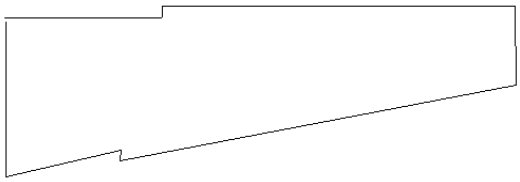

Figure 5.10: Schematic figure of the web plate before the flanges with different thicknesses are attached in Vårby Bridge

To get a model with the correct behaviour .i.e. the flanges are connected in their respective end nodes, the web plate was sketched with a straight top and bottom edge, Figure 5.11. The height of the web near the supports (left end in figure 5.11) was increased in order to adjust for that the top flange in this area is 2 times thicker. The web plate are sketched using the height of the vertical web stiffeners as reference, so this increased height at the end of the web plate will only affect the first section between the end and the first vertical web stiffener. The thicker part is given the correct stiffness by using an offset ratio of 0.024, i.e. the centre of gravity is moved slightly downwards. By means of this, the top surface is a straight line after the flanges are attached to the web plate and the shell elements are attached in the same node. The change in stiffness due to that the cut out areas for the bottom flange are represented by a straight line are neglected.

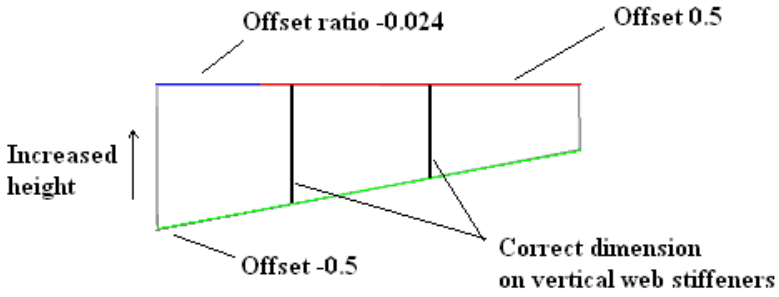

Figure 5.11: Schematic figure over how the flanges are attached to web plate using altered offsets. The figure shows the part "Steel 3" containing two vertical web stiffeners

The changes in second moment of inertia for the main girder due to these small geometrical changes are negligible and will not influence the global behaviour.

5.7.2 Bridge dimensions

Each main girder in Vårby Bridge is erected from 12 structural members, denoted in Appendix A, 1-12 followed by C or D depending on which main girder it belongs to. Main girder C and D for every number (1-12) have the same shape and geometry except for some of the vertical web stiffeners, were the height differs 1-2 mm. From these 12 structural members (including C and D) 4 main types can be seen. The 4 types have the same geometrical shape but with a slight difference in the dimensions, see Table 5.4.

Table 5.4: Summarising table over the diverging dimensions for top and bottom flanges in the main girders in Vårby Bridge, the members with bold text are used in the bridge model

Structural member	1CD	**2CD**	3CD	4CD	5CD	6CD
bf	28 47	**47** **50**	39 50	39 45	42 45	42 47
tf	20	**20** **47**	20 47	20 41	20 41	20 42

[mm]	**7CD**	**8CD**	9CD	10CD	11CD	**12CD**
bf	**42** **47**	**42** **47**	38 47	38 50	46 50	**28** **46**
tf	**20** **42**	**20** **42**	20 42	20 47	20 41	**20**

In the bridge model 4 different parts are used (denoted with bold text in Table 5.4), each part consisting of two main girders with the same geometry. Steel 1 and 3 are created using the geometry for the span between support 5 and 6 (drawing 8CD and 7CD). Steel 2 are created using the same geometry as in steel 1 but with 3 diaphragms instead of 4. Steel 4 are created from drawing 12CD and also cover 1CD. Steel 1 includes 4CD, 6CD, 8CD and 10 CD. Steel 3 includes 3CD, 5CD, 7CD, 9CD and 11CD

The geometrical differences within the structural members in the main girders in Vårby Bridge are negligible and the approximation to use steel 1-4 when constructing the bridge model does not affect the global behaviour.

5.7.3 The connection between diaphragm and main girders

In the Vårby Bridge the diaphragm beams are attached to the vertical web stiffener with bolts, see figure 3.2 and 3.4 in chapter 3.2, and the diaphragm beams have cut out areas which can seen in Appendix A; figure 9.5:C414 and in figure 9.10. In Abaqus, the edge of the web in the end of the diaphragm beam is attached to the edge of the vertical web stiffener of the main girders.

This approximation makes this connection stiffer due to that the diaphragm beam and the vertical web stiffener are merged together. But due to the large number of heavy bolts in this connection and that only the web is connected to the vertical web stiffener in Vårby Bridge, this approximation in the bridge model is acceptable.

5.7.4 Global location of the main girders

Due to the road building of the highway that passes Vårby River, the Vårby Bridge is shaped in a certain way. The top surface in the bridge is also somewhat higher in the spans to compensate for the self weight. In Abaqus the bridge is modelled with the two main girders starting in the same level, separated by the designated transversal distance. The top surfaces in the main girders are modelled as a horizontal line.

These approximations do not have any influence of the static behaviour of the bridge model.

5.7.5 Connections between the concrete deck and the top flanges

In Vårby Bridge, studs are used in the connection between concrete deck and the top flanges. In Abaqus the connection is modelled with a “tie constraint” meaning that the adjacent areas are bonded with full interaction in all degrees of freedom. The tied connection is overestimating the interaction; it will not take any slip between the adjacent surfaces into account, a possible elongation of the studs due to the uplifting force is neglected and the deck are prevented to lift away from the top flange in the main girders.

The tied connection are however acceptable in the global analysis when the structural behaviour of the bridge is studied.

5.7.6 End-diaphragms

In Vårby Bridge both of the end-diaphragms, S1 and S7, are adjusted due to the connection between the bridge and firm ground which can be seen in Appendix A; main girder 1 and 12cd. In Abaqus, the end diaphragms are modelled without the cut out area and with the transversal beam placed at the same distance from the top as in the other diaphragms in the bridge model (400 mm).

This was done do make it easier to create the parts for the end sections and the change in geometry will not influence the global behaviour of the bridge model.

5.7.7 Concrete deck

The thickness of the concrete deck in Vårby Bridge varies along the width; see figure 3.5, chapter 3.2, and the end beams do not have the same geometry. The thickness is approximated in Abaqus with an appropriate number of strips along the deck where the height of each strip is an average of the maximum and minimum value in the strip. The end beams are modelled with an equal width and height and the dimensions are approximated from the drawings.

The concrete deck is assumed to be un-cracked (State I) and therefore is a static analysis performed in Abaqus. The deck is also modelled without any reinforcing bars and with the same modulus of elasticity in the whole deck.

5.8 Verification of the global bridge model

The verification of the bridge model was made by comparing the stresses in the global channels from the on-site strain measurements with the corresponding values obtained in Abaqus. In addition to the comparisons, the deformed shape from the analysis for each traffic lane were reviewed ocular to verify that the structural behaviour were as expected. Figure 5.12 visualize the bridge model when loaded in right lane at a certain step.

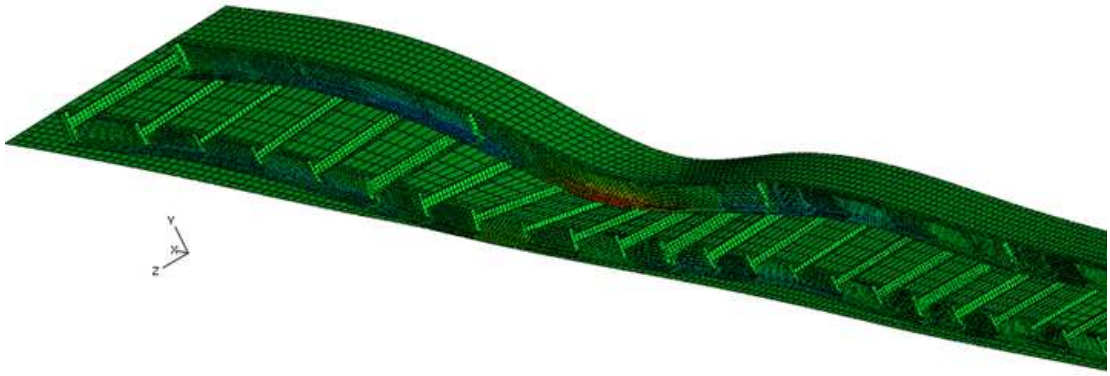

Figure 5.12: Moving load in right lane, passing diaphragm F23 which gives the maximum stress in global channel 8

The global channels, Ch 4 and 8, where the strain measurements are compared to the values obtained from analysis are located at diaphragm F23 on the lower surface of

the bottom flanges in the main girders. The global channels can be seen in figure 3.10, chapter 3.4.1.

Measurement strain data were collected from right, left, mid- and the outer traffic lane and these were plotted against the corresponding values from the analysis. Figure 5.13, Figure 5.14, Figure 5.15, Figure 5.16. The truck used during the measurement was travelling when measuring the right- and outer lane at a speed of 30 km/h, in mid lane at a speed of 50 km/h and in left lane at a speed of 90 km/h.

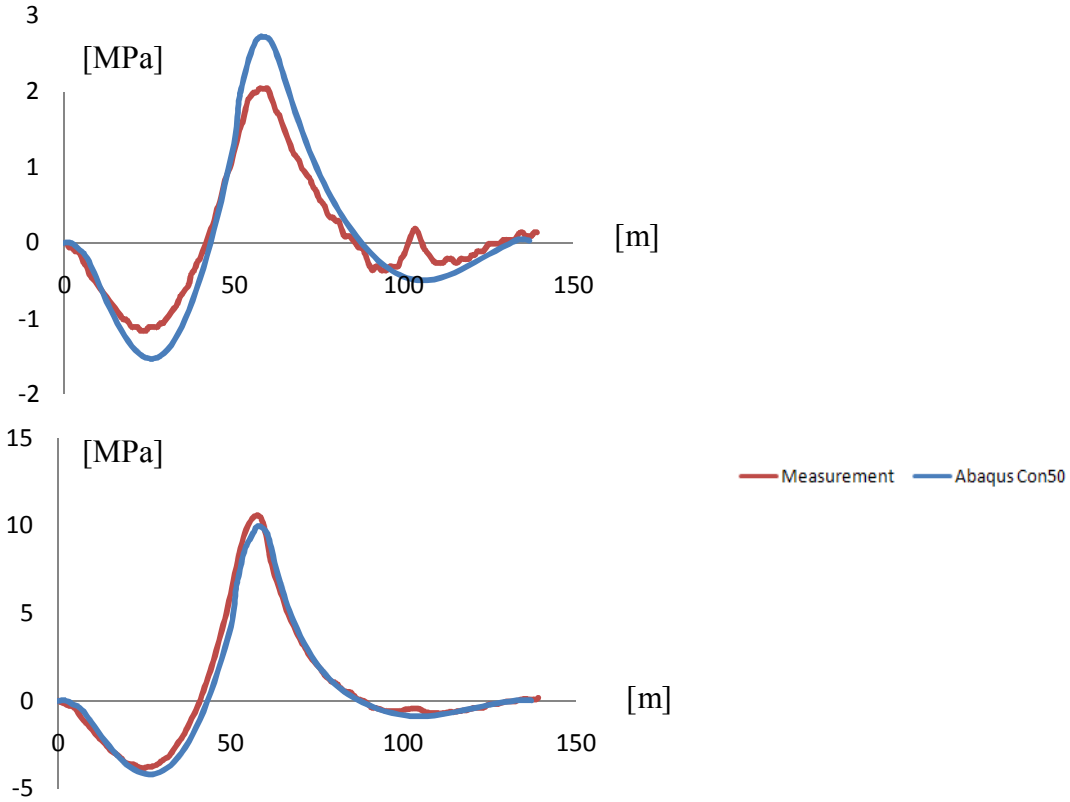

Figure 5.13: Right lane Ch 4 and 8

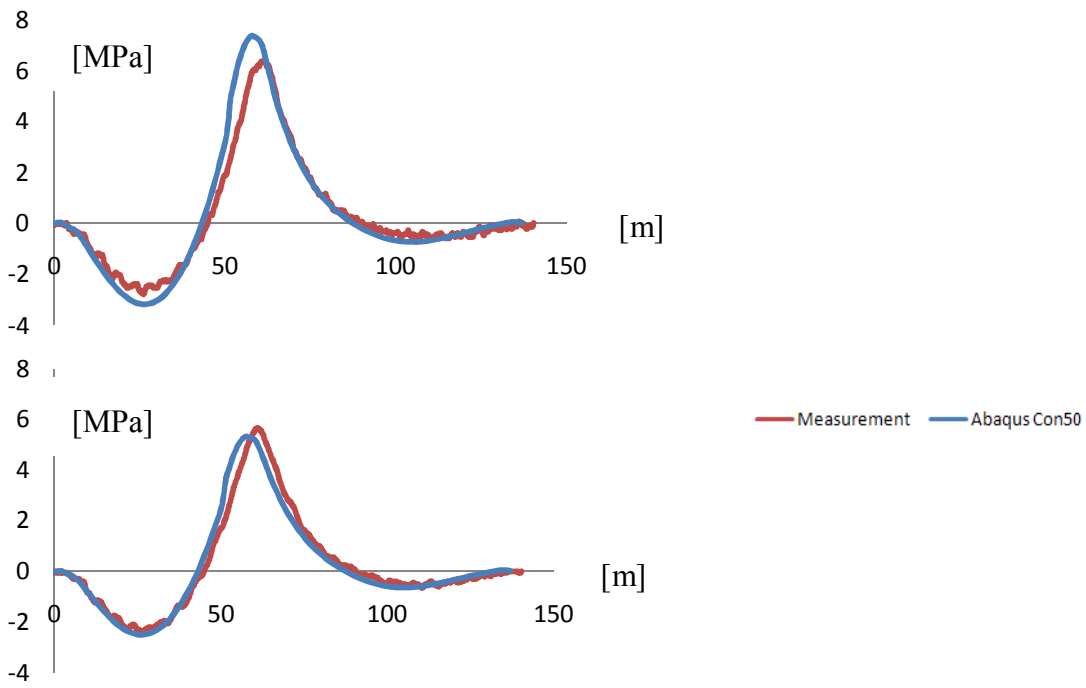

Figure 5.14: Mid lane Ch 4 and 8

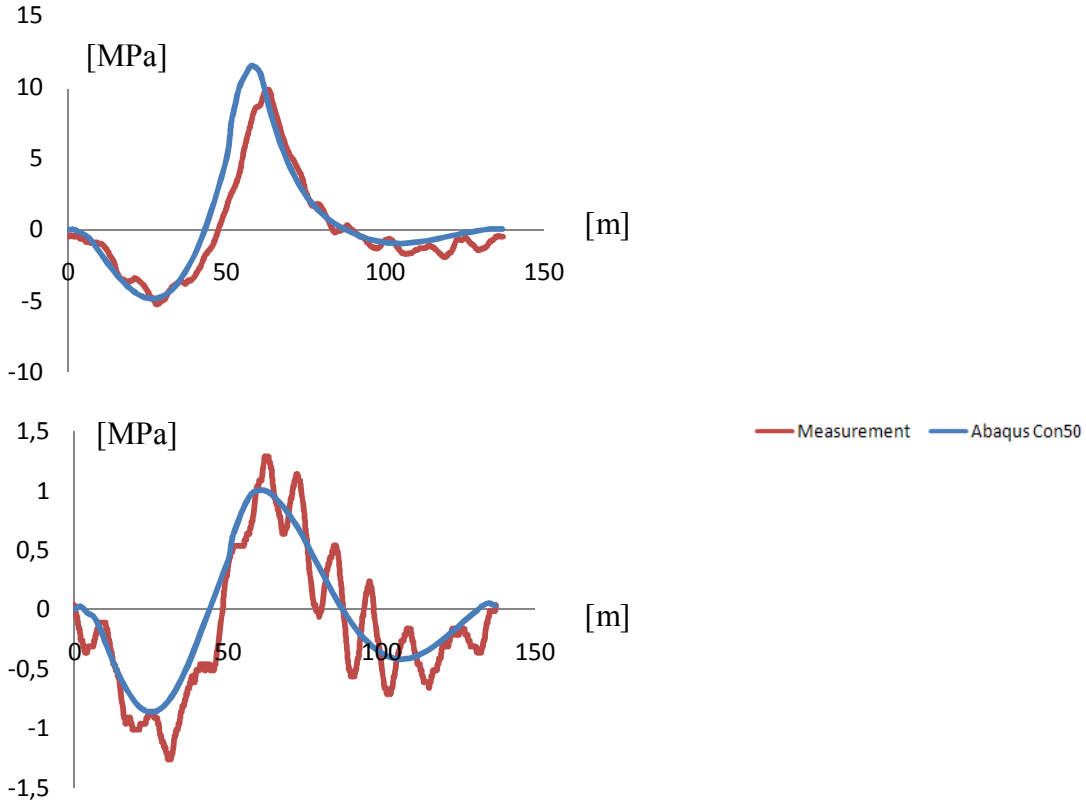

Figure 5.15: Left lane Ch 4 and 8

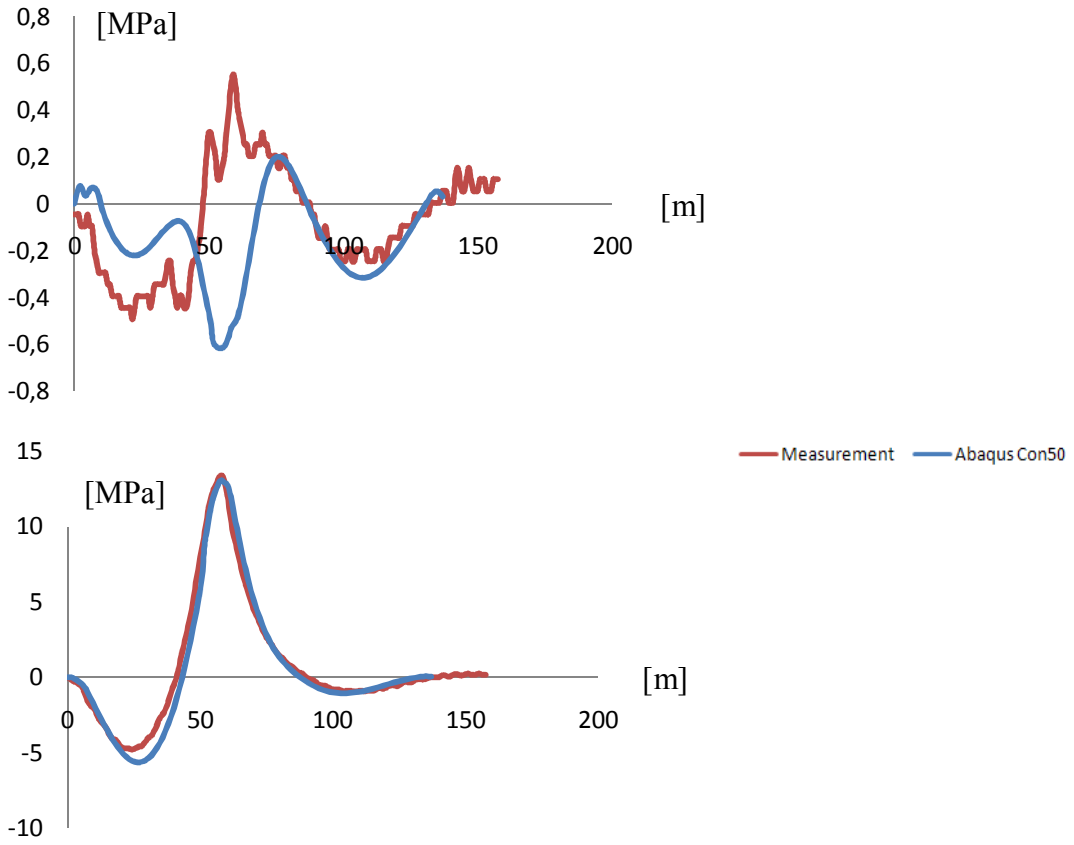

Figure 5.16: Outer lane Ch 4 and 8

Overall there is a good agreement between the on-site measurements and the values obtain in analysis. The shapes of the curves match each other quite well with top and bottom values on the same positions although with diverging values in some cases. As can be seen in figure 3.14, chapter 3.4.2, the global channel 8 are located at the main girder under the right traffic lane and global channel 4 under the left lane. However, as can be seen in the figure, the traffic lanes are not symmetrically arranged on the concrete deck which leads to that channel 4 are further away from left lane then channel 8 are from right lane. Below comments about each traffic lane are presented.

- *Right lane* Channel 8 agrees well, the analysis values in channel 4 are higher than the measurement values which means that more load have been transferred to the opposite side in the bridge model compared to values from on-site measurements.

- *Mid lane* Channel 8 agrees rather well, and as above, the analysis values are higher than the measurement data for channel 4. The top and bottom values from the measurement data are almost identical which could indicate that the truck in the on-site measurement run very close to the centre line of the bridge, while the analysis show higher values for channel 4 which is reasonable because the mid lane are closer to channel 4.

- *Left lane* The measurement data from channel 8 is irregular; the reason could be that the truck run in 90 km/h and creates thereby a dynamic effect. The two curves follow however the same pattern but it is uncertain if that measurement is reliable since it is small stresses. The analysis values for channel 4 are

higher than those from measurements who show almost the same values as channel 8 when loaded in the right lane. This is surprisingly due to that the left lane is placed partially outside the main girder, on the console, and more loads should go to this strain gauge (channel 4) than if the load is placed inside the main girders (which is the case for right lane).

- *Outer lane* The outer lane is located outside the right main girder and the majority of the load goes to channel 8 which can be seen in the curves who match very well. The value for channel 4 is very small and is fairly needed in the comparison.

Adding together the comparisons for each traffic lane with the ocular judgment of the deformed shape a good picture of the performance of the bridge model are established. However, further research was performed by a parameter study to ensure the correctness of the bridge model. (The main reason to the parameter study was due to the fact that channel 4 consequently showed higher values from analysis compared to these from the measurements).

Due to the observations mentioned above, it is possible that the given geometry received for the concrete deck in Vårby Bridge (width of each traffic lane and location on deck) is approximated values. By reason of the suspicious that the given widths of each traffic lane maybe not are correct, an analysis with reduced number of load steps were perform in the right lane. 9 load steps were moved 100, 200- and 500 mm towards the outer lane in transversal direction i.e. away from the centre line of the bridge. Stresses in both Ch 4 and 8 were collected and compared to the strain measurements from Vårby Bridge but also with load in original position (one bogey wheel in location directly over right main girder and the other bogey wheel between the main girders) Table 5.5.

Table 5.5: Sensitivity when the load is moved in 100, 200- and 500 mm in transversal direction, right lane

	Measurement	Original position	100 [mm]	200 [mm]	500 [mm]
Ch 4 [MPa]	2,03	2,72	2,60	2,48	2,12
Ch 8 [MPa]	10,56	9,98	10,10	10,22	10,57

The table show that when the load are moved 500 mm in transversal direction, which means that the resultant of the truck load are moved closer to the right main girder, the values from Abaqus are in close proximity to the values from the strain measurements.

The sensitivity of the load location was further investigated by changing the distance between the wheel tracks in transversal direction. The original distance were compared to a larger distance, see Appendix D. The difference between the two wheel tracks distances was negligible.

The load where also moved to the mid span in transversal direction to check the symmetry of the bridge model; the main girders have the same geometry and the deck are laterally transposed around the centre line in longitudinal direction. The curves for

Ch 4 and 8 were plotted against each other and showed identical results; see Appendix D.

Due to the approximation that the diaphragm beams are merged to the vertical web stiffeners in the bridge model, an analysis when the stiffness of the diaphragm beams is decreased was performed. The goal was to see what influence the diaphragm beams have for the global behaviour of the bridge model. The comparison showed that there were no difference for the stresses in Ch 4 and 8 when reducing the diaphragm beam stiffness markedly, see Appendix D.

The influence of different young´s modulus for the deck was investigated by changing it from 20 to 70 GPa, were 50 GPa was the original value. This was made for the right traffic lane and the plot is visible in Appendix D. The plot showed that a more stiff concrete deck transfer more load in the transversal and longitudinal direction of the deck compared to a deck with lower stiffness.

During analysis of the results the tensile stresses in the concrete deck were checked. The maximum value reached was 1.4 MPa and the concrete deck was kept in the assumed state I.

Summing up the verification above, the global model established is representative for the performance of Vårby Bridge in the field of interest for this master thesis.

6 Refined model

6.1 Introduction

With the global model established and verified the next step was to model the area of interest in a better way since the mesh, application of loads and also shell elements may be too coarse to capture the local effects. Refinement of the model could be done in various ways, for instance the area of interest can be made as a sub model which might consist of solid elements with fine mesh but still keeping it rather small considering computer usage time. As input, outcomes from global analysis should be applied on the sub model to get correct results. Another alternative is to use the global model and try to make a fine mesh in the area of interest and also apply the loads in a different way. This thesis used the later proposed alternative since the saving of time was crucial, a sub model would have taken too long time to create.

The actions taken to refine the model were to make a finer mesh and changes how the loads were applied. The element size of the mesh was decreased from 250 mm to 25 mm in the span where the measurements were performed. The load was applied making areas of 0.2x0.6 m modelling the 6 tyres of the truck and using pressure load instead of concentrated forces. 5 load steps were chosen to make it possible to capture the highest stresses in the interesting area.

6.2 Comparison between refined model and measurement

The results from the refined model were then compared to the on-site measurement data; one measurement from each lane was used. Data was taken from channels 1-3, 4-6 and 9-10 at the span section and channels 12-15 at the support section. Due to the changes of the mesh the nodes corresponding to channel locations could be found in the model, which was not the case before since the mesh then was too coarse. The changes in application of the loads were also beneficial obtaining a better stress distribution, though the difference was not large.

The difference was large between measurement data and results from Abaqus when comparing, Table 6.1. All models, right, mid and outer lane, had the same behaviour, but with difference in magnitude of stresses, which indicated that something was not properly modelled.

Table 6.1: Results from comparison between Abaqus and measurements, right lane. Only values from channels on one vertical stiffener is presented since both sides experienced the same behaviour

	Ch 5 [MPa]	Ch 6 [MPa]	Ch 7 [MPa]
Abaqus	-26	-17	-12,5
Measurement	-9,0	-3,0	-1,5

Several things influenced the results and the ones considered were:

- The stiffness of the diaphragms and how they were connected to the vertical stiffeners
- How the stiffeners were represented with regard to the stiffness

- The possibility that it was a local problem at the top corner of the stiffener on the diaphragm side where it could be a large stress concentration due to the top flange bending over the corner
- A poor modelling of the composite action between the I-girder and the concrete deck

The diaphragms were ruled out due to the comparison with channel 9 and 10 showed good agreement with the result from measurements compared to Abaqus in all models, Figure 6.1. When looking at the stresses in the stiffeners and especially the principal stresses the distribution was as expected with only one principal stress near the edge of the diaphragm side and no shear stresses. The possibility that it was a local problem causing too high stresses further down in the stiffener was rejected, even though a stress concentration of large magnitude was found. The area of the high stresses was though indeed local at the corner and faded out before reaching the nodes of interest. The problem with the model, which had been of great concern since starting the modelling in the thesis, was the modelling of the composite action. Globally it worked very well, which was seen in previously chapter, but when looking locally the forces in the studs were of great significance.

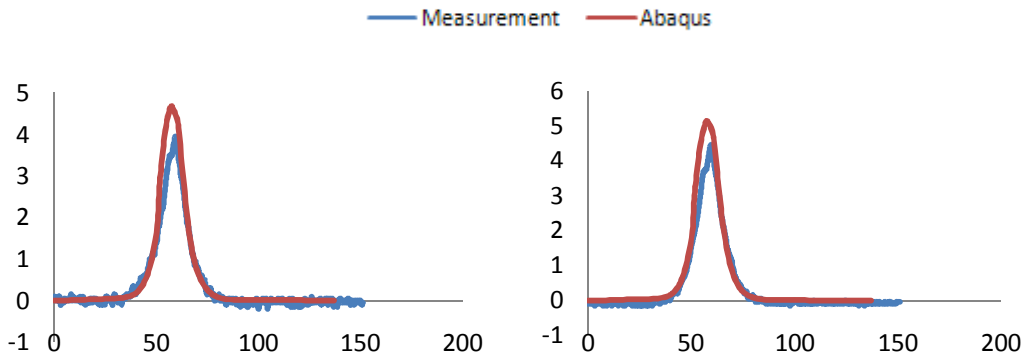

Figure 6.1: Influence lines for channel 9 and 10, mid lane

Since the studs were placed in pairs at the bridge one of the studs were loaded in tension and the other in compression creating a force couple. This force couple had large influence on the stresses in the stiffener. The composite action was modelled as previously said with tie constraints between the entire width of the top flange and an equal width at the deck. This worked incorrectly and probably the cause for unsatisfying results in the local comparison.

To solve the problems two approaches was formed; approach 1 was to change the model not using tie constraints and try to make a better representation of the composite action. The other approach (2) was to keep the model but move the application of the loads in order to make the use of tie constraints work.

6.3 Approach 1

To model the studs more appropriate the suggestion was to use axial springs, which was in-built parts in Abaqus. The idea to use springs was to model the studs experienced in tension and that they should not influence the structure when compressed. When compressed they should not make an influence since the concrete deck would put pressure on the I-girder below using contact surfaces. These new

properties of the model were done in the span where the comparisons were made. When trying this it did not work as planned, the springs did not compress and overruled the contact surfaces of the top flange and the concrete deck, causing strange results. The contact surface was made to function such that a gap could appear between the concrete deck and the main girder, this would appear on the side where the studs were in tension, but then closing when the studs where released from tension.

The next step made was to keep the contact surfaces but take away the row of studs that were compressed keeping only the studs in tension to take away the errors with compressed springs. Still no good results were obtained and one other possibility to solve this was found. All the above tests in approach 1 were with the truck modelled in the right lane which could cause difficulties in interpretation how the distribution would be. In other words, were the studs really in tension? To ensure this the truck was modelled driving in the mid lane, which would mean that the studs were in tension.

The result from the last model was none; it ended up with convergence problem and no solution. Probable causes for this could be that the springs and contact surfaces were placed in a too small area of the bridge model and had to be increased. The area was increased and the model tested in several steps until the area was the entire bridge. Despite all the efforts put in still no convergence nor solution and the approach to change the model was abandoned.

6.4 Approach 2

The second approach was to use the model with refined mesh and tie constraint. To get different results compared to earlier models the position where the load was applied were changed. As shown previously in the report the use of tie constraints worked well for global studies of the bridge but not locally, since the composite action comes into play. The main problem suffered with the first approach was how to model the force couple created when the concrete slab rotated, i.e. the composite action.

Knowing that the tie constraint worked well under the influence from pressure, the load was moved to a position more to the right of the original position when modelling a truck in the right-lane. This was done since earlier, from the global analysis; it was known that the results were sensitive when moving the application of load transversally on the bridge. With regard to that the aim was to get the entire right upper flange in compression and obtain better results without needing to model the composite action in two directions.

The load was moved from the original position to the right with 500 and 650 mm showing the results in Figure 6.2.

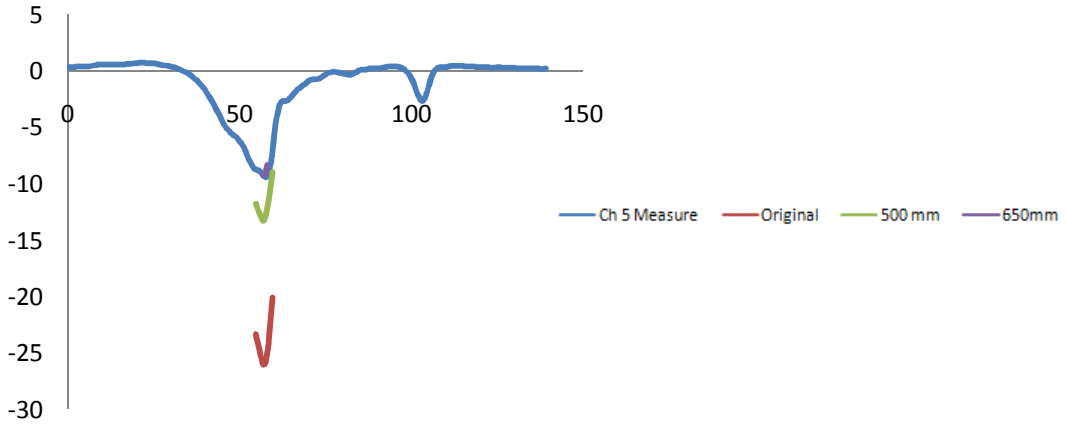

Figure 6.2: Sensitivity of stresses channel 5 when moving load tranversally

Channel 1 experienced the same behaviour as channel 5 and the results confirmed, as for the global analysis, the sensitivity when moving the load transversally. Also, the results presented above came quite close to the measured values. When looking on results from the other channels, on the vertical stiffeners, they experienced the same behaviour, coming closer to the measured values. However, the decrease in stresses was not as large as for the highest placed channels, meaning that the stress distribution in the vertical stiffeners still was not properly modelled.

The results from the support were similar in behaviour as the span models, but the changes in magnitude of stresses were not as large. In Table 6.2 the difference in sensitivity between span and support is presented.

Table 6.2: Difference of sensitivity when moving load in transversal direction, right lane. Comparison between the corresponding values in support and span

	-300 [mm]	0	500 [mm]	650 [mm]
Ch 5, span [MPa]	-33,0	-26,0	-13,3	-8,3
Ch 12, support [MPa]	-26,6	-22,2	-13,5	-10,

7 Conclusions

The questions to answer in the thesis were; why do the fatigue cracks occur and why only in span? Also how the cracks should be retrofitted were a task stated.

The results from the refined modelling phase were not as good as hoped for. The modelling of the composite action was not solved and the stress distribution obtained was not good either. However, based on the results collected and the comparisons made with measurements one theory have been formed on why the cracks occur.

When comparing the results from the models with the measurements there are not good agreement when looking at the magnitude of the stresses. When looking at the behaviour there agreement is very good, which means that the results can be of use in comparisons between values from the models since they have the same modelling errors.

The first approach when drawing conclusions was to see how high stresses that the bridge experienced from the measurements. Even though residual stresses exist there is no sign of any stresses reaching the levels of stress range causing fatigue cracks. Residual stresses must be a part of causing the fatigue cracks since the area where the cracks are formed is loaded only in compression. This was confirmed when looking on where the traffic lanes are located on the bridge.

Previously in the report a summary of the literature study was made. In the summary four different theories that could cause fatigue cracks were proposed. Below figures describing each theory and conclusions of what influence they have for inducing fatigue cracking in Vårby Bridge are presented.

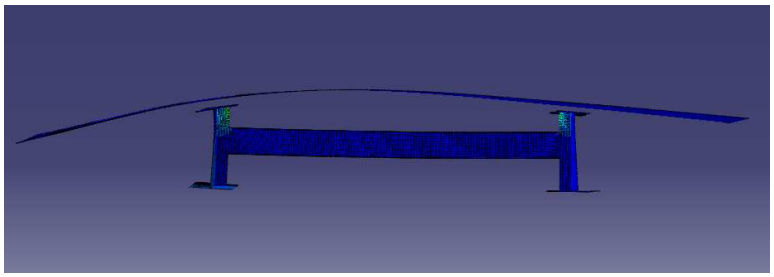

Figure 7.1: Hogging moment created whit vehicles driving in outermost lane (on the outside of the main girders). The hogging moment then creates high tensile stresses in the area where the fatigue cracks occur.

Hogging moment (Figure 7.1) can occur if there are vehicles on the outermost lanes, but the stresses are not that large and the number of cycles is very small, since these lanes are not intended for traffic.

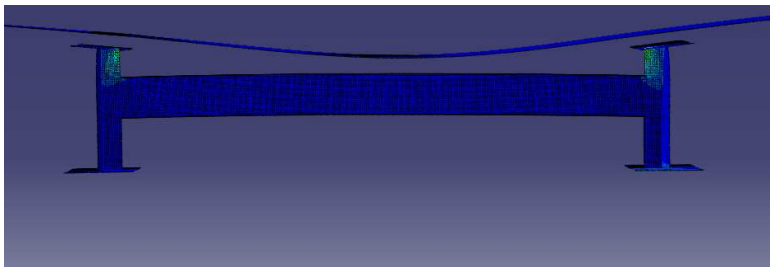

Figure 7.2: Rotation of the concrete slab which occurs with vehicles driving between the main girders which influence compressive stresses at the vertical stiffener. In itself this cannot cause fatigue cracks, but together with residual stresses in the

The rotation of the concrete slab (Figure 7.2) will occur but does not create magnitudes of stresses which leads to formation of fatigue cracks and the same yields for the last two theories presented (Figure 7.3), (Figure 7.4). To be noticed however is that the highest stresses are found when placing the load directly above the area of interest.

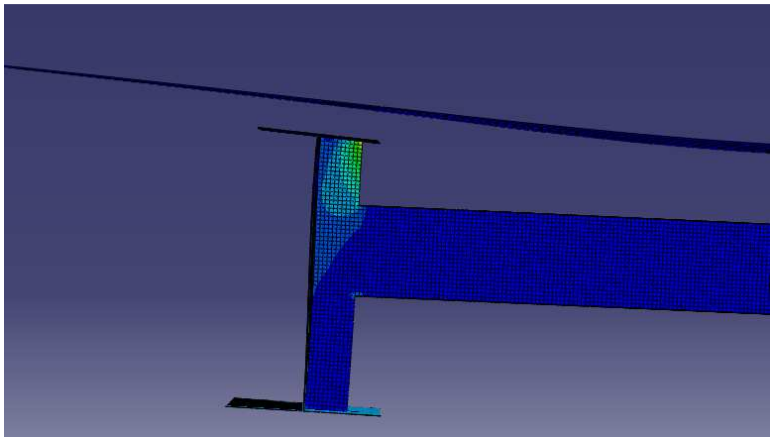

Figure 7.3: When vehicles drive directly above the vertical stiffener causing compressive stresses together with the residual stresses fatigue cracks may form

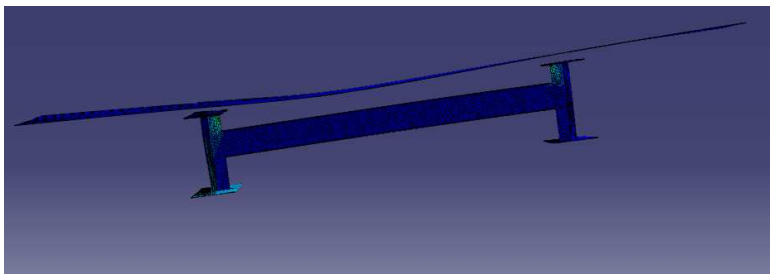

Figure 7.4: The bridge rotating around one main girder. This might happen as a consequence if the main girder, with load applied directly above, suffers from large deflection. This could influence a rotation around the other main girder causing compressive stresses at the welded joint.

7.1 Theory of why cracks have occurred

The theory we present what might have caused the cracks were created when comparing results from the models. When looking on the sensitivity when moving the load transversally in the near of the main girder there was one difference found between span and support.

The sensitivity is larger in the span compared to the support which might depend on the double vertical stiffeners at the supports. This is not something that can be found in the measurements from the bridge, but might still be valid. When doing the global analysis we actually stated that the data we got of lane locations were wrong. When comparing load location from our global and local analysis we found that the location when the measurements and the results coincided the best was about the same for both analyses. This leads to the conclusion that during the measurements the most severe loading case can have been missed.

We think that the fatigue cracks are caused by vehicles driving directly over the area of interest with one wheel and the other between the main girders. If any other vehicles would be driving on the bridge at the same time this is beneficial for the cracks forming, since the compressive stress will increase. With this theory presented it can be stated that the theories dismissed above will also influence.

The main cause is the one mentioned above, but there is a mixture of effects leading to the large number of fatigue cracks. All the other theories, except hogging moment, will amplify the magnitude of stresses if these occur at the same time, for instance when one vehicle is in the right lane and another vehicle in the mid lane causing larger rotation of the concrete slab. Also the residual stresses play an integral part since these make it possible for fatigue cracks to be formed in compression.

With this theory presented above the question of why fatigue cracks only occur in span and not at support can be answered. This has not been confirmed in the report since the model is not fully correct. The answer to the question is perhaps no answer or that we cannot know. The support section might suffer from damageable stresses but lower than the ones in the span which then demands more cycles for fatigue cracks to be formed. The stresses might be low enough such that no damage will occur. The important to point out is that cracks may occur at support also.

Since we do not have confirmed the theory fully, no investigation in retrofitting methods has been performed.

7.2 Further studies

To confirm the theory presented more work needs to be done. First of all a complete model must be formed, especially to model the composite action properly is of essence. The actual stiffness of the concrete would also be of interest as input for the models. Retrofitting methods need to be evaluated since, if the theory is correct, there is a mixture of effects causing the fatigue cracks.

Since the aim of this thesis were to model the bridge and compare results with measured data no regard of the measured data itself has been taken. Evaluation and calculation of stress levels from the measured values should be performed.

A new measurement of the actual bridge would be very good if possible. The input from the measurements to this thesis was not good not giving the correct measure conditions, loading positions or position of lanes.

8 REFERENCES

Chung, W., & Sotelino, E. D. (2006). Three-dimensional finite element modeling of composite girder bridges. *Engineering Structures , 28*.

Eriksson, K. (2009). *Materialprov från vägbro i Vårby.* Luleå: Luleå Tekniska Universitet.

Greiner, R., & Taras, A. (2009). *Fatigue failures at stiffener connections in highway composite bridges.* Graz, Austria: Graz University of Technology.

James, G., & Kärrfelt, U. (2009). *Bro över Vårbyfjärden: Sprickor i avstyvningar.* Projektengagemang i Stockholm AB, Anläggningsunderhåll, Stockholm.

Okura, I., Shiozaki, T., Fukumoto, Y., & Nanjyo, A. (1995). *Stud arrangement to reduce fatigue cracking in vertical stiffeners.*

Sakano, M., Kawakami, Y., Sakai, Y., & Matsushita, H. (2007). Retrofitting method against fatigue cracking in welded joint between steel deck and vertical stiffeners. *Pacific Structural Steel Conference 2007, Steel Structures in Natural Hazards.* Wairakei, New Zealand.

Appendix A: Drawings of Vårby Bridge

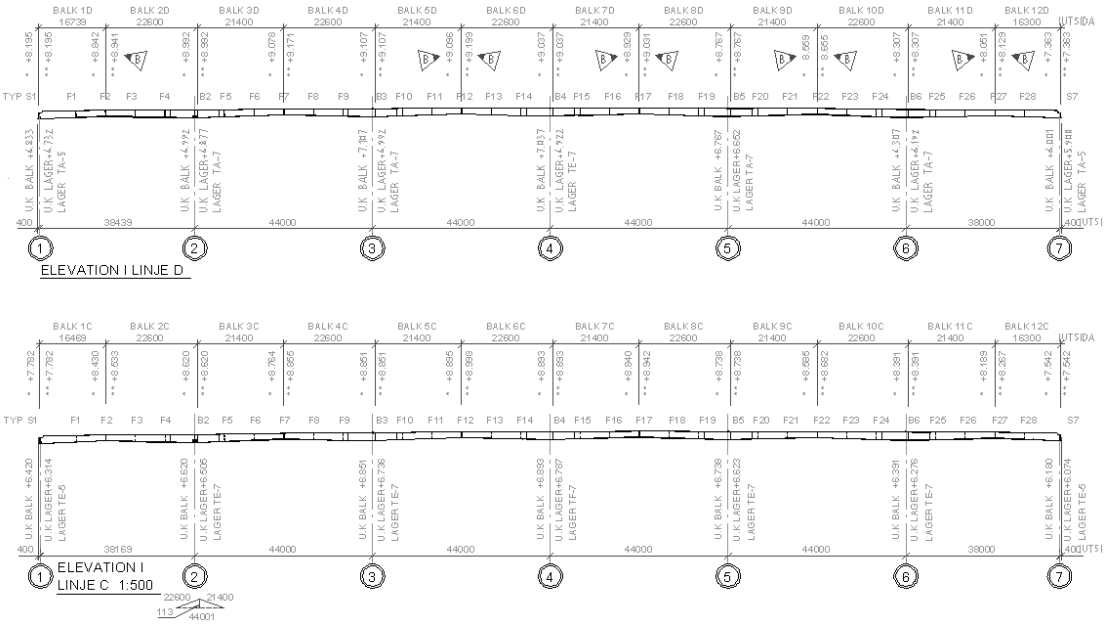

Figure 8.1: Elevation of the two main girders

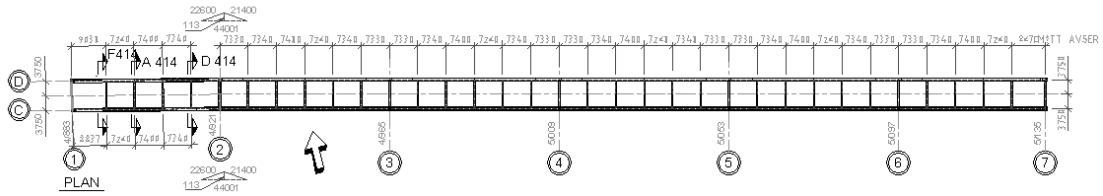

Figure 8.2: Plan of the two main girders

Diaphragms in Vårby Bridge

In Vårby Bridge there are three types of diaphragms in the spans, one type representing the end diaphragms and one type for the intermediate supports. Figure 9.3, 9.6-9.8 and 9.12 show were in Vårby Bridge the diaphragms are located. The height of each diaphragms (F1-F27, B2-B6 and S1, S7) can be seen in the drawings showing the main girders.

Diaphragms in span (type 1,2 and 3)

The different types of diaphragms in the spans have the same geometry except for the height that differs depending on where in the spans they are located.

Type one

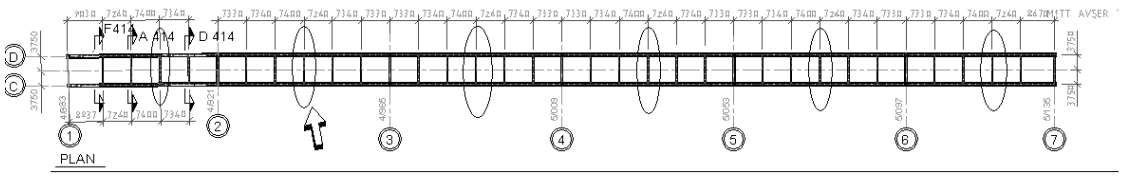

Figure 8.3: Type 1, diaphragms F2 F7 F12 F17 F22 F27

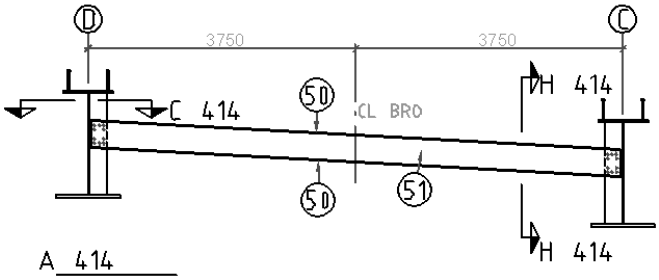

Figure 8.4: Cross-beam 51: web 12x370x7420, flanges 14x350x7420

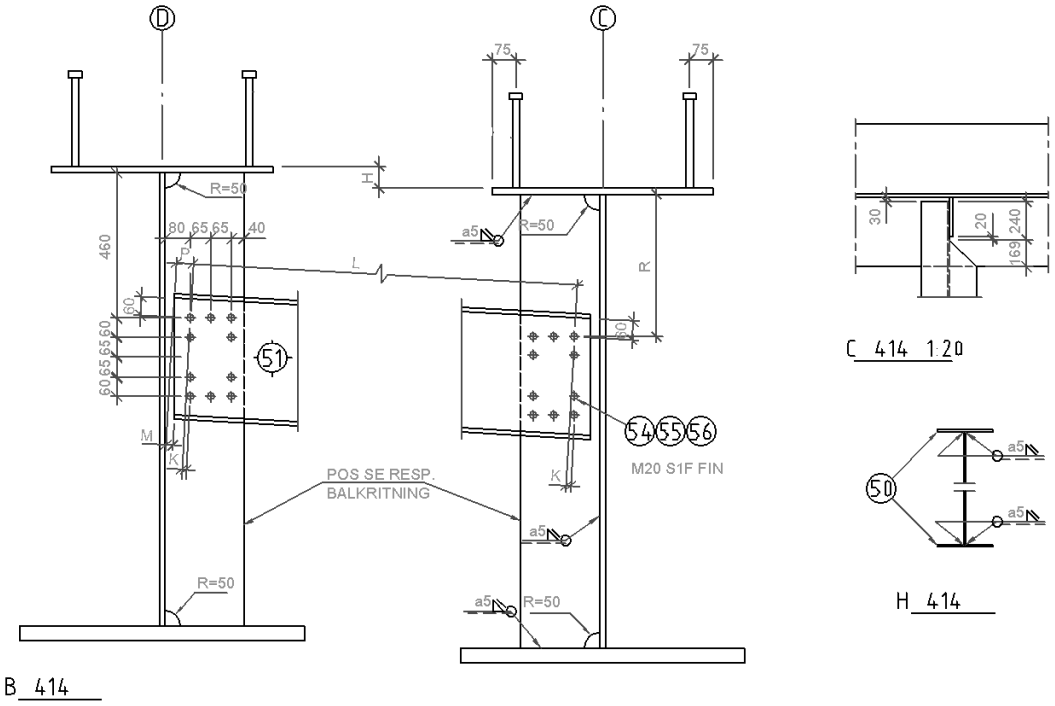

Figure 8.5: B414 Section of the bridge (type one) showing the two main girders and the cross beam in span, C414 Plan view of the cross-beam with a modified top flange in order to fit the vertical web stiffener in the main girder, H414 Section of the cross-beam with the fillet welds

Type 2

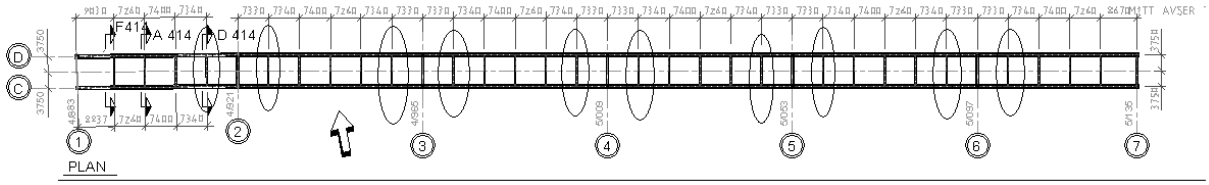

Figure 8.6: Type 2, diaphragms F4 F5 F9 F10 F14 F15 F19 F20 F24 F25

Cross-beam 53, web 12x710x7420, flanges 14x350x7420

Geometry same as for cross beam 51

Type 3

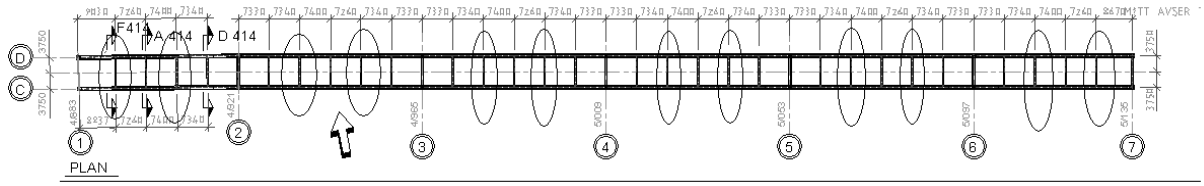

Figure 8.7: Type 3, diaphragms F1 F3 F6 F8 F11 F13 F16 F18 F21 F23 F26 F28

Cross-beam 52, web 12x540x7420, flanges 14x350x7420

Geometry same as for cross beam 51

Diaphragm in end supports (S1, S7)

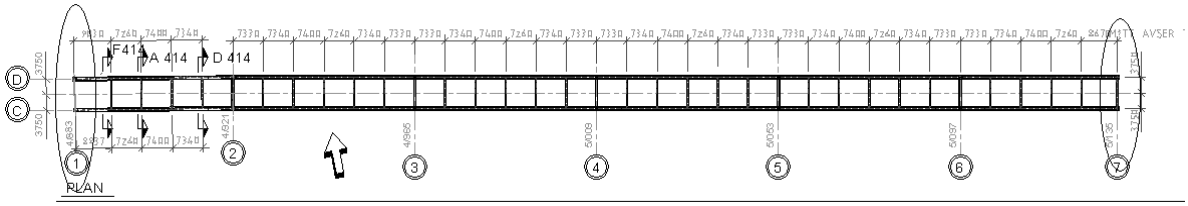

Figure 8.8: Diaphragms in end support S1 and S7

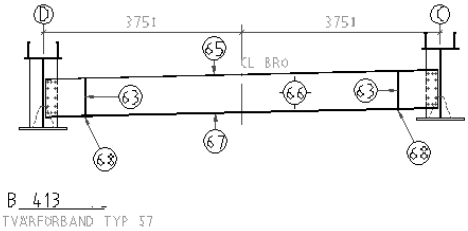

Figure 8.9: Cross-beam 66, web 12x700x7442, top flange 15x300x7424, bottom flange 20x400x7424

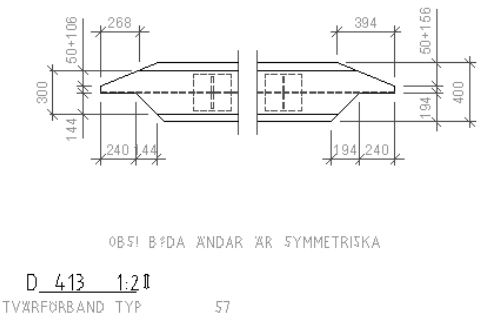

Figure 8.10: D413, Plan view of the cross-beam with the cut out areas in the cross beam

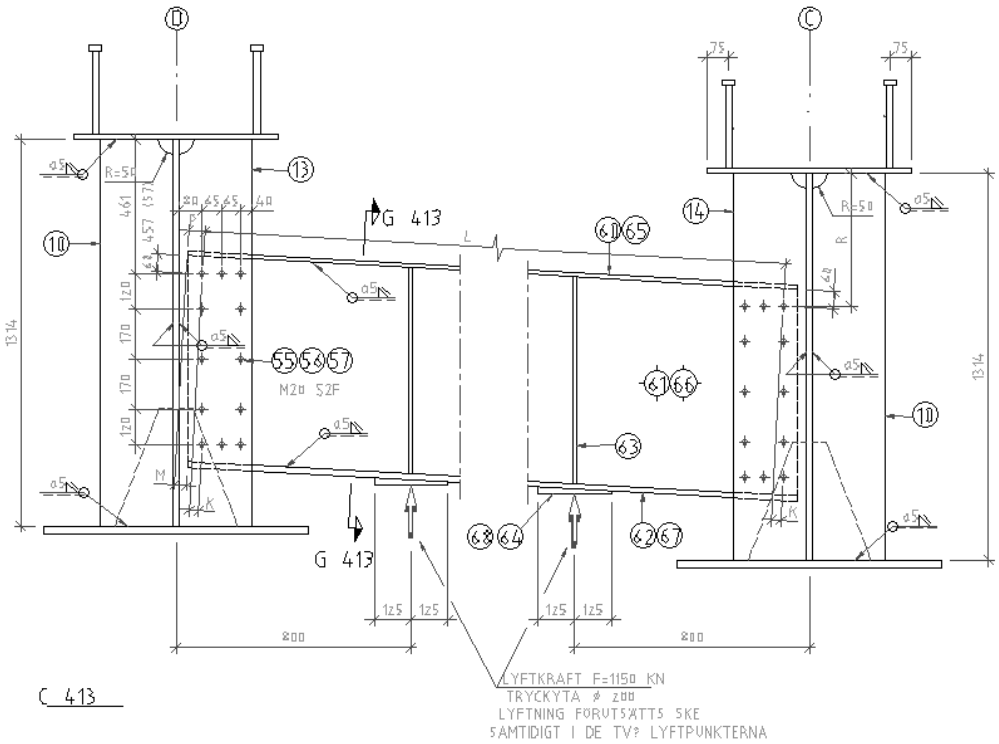

Figure 8.11: C413, Section of the bridge at end support S1 and S7; Vertical web stiffener marked with (10),(13),(14)= 25x250

Diaphragms at intermediate supports (B2-B6)

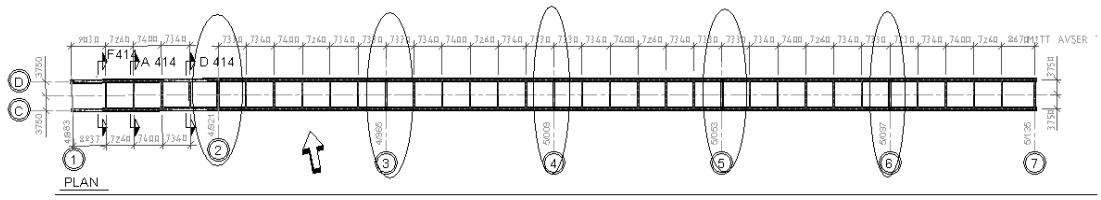

Figure 8.12: Diaphragms B2, B3, B4, B5, B6 at intermediate supports

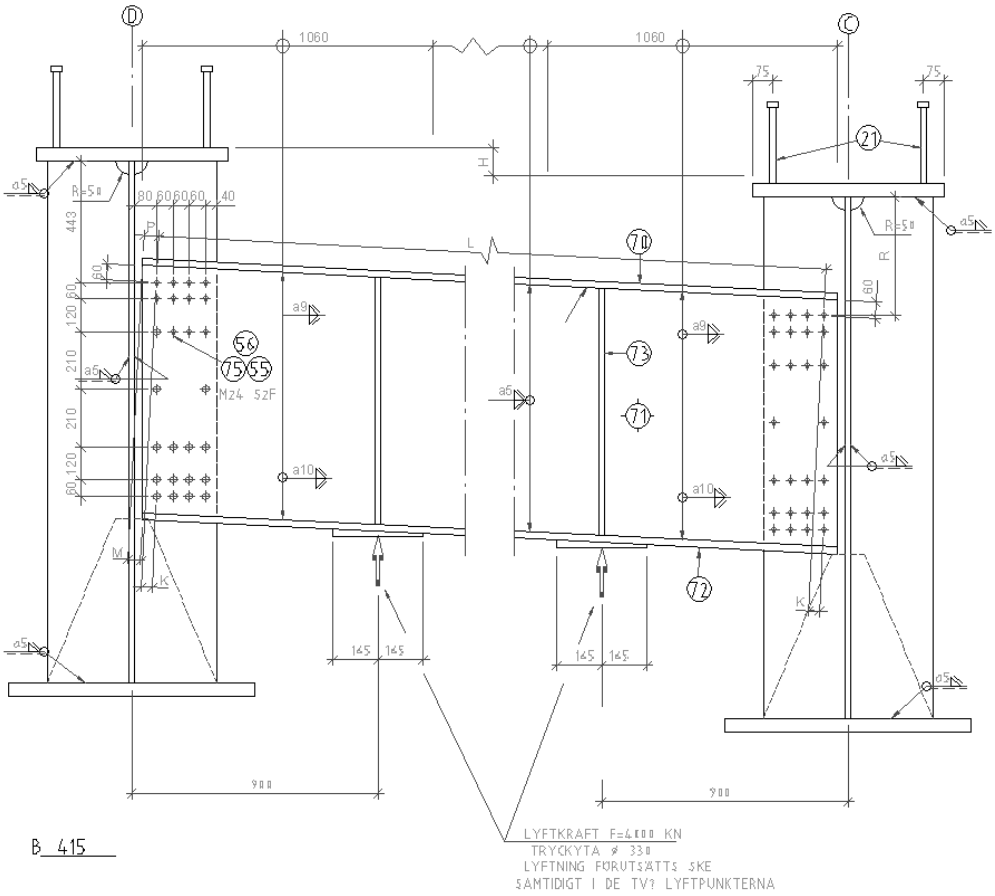

Figure 8.13: B415, Section of the bridge at intermediate support B2-B6; Vertical web stiffener, 25x300

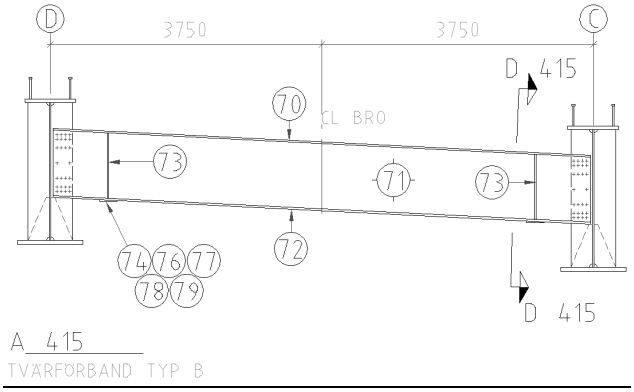

Figure 8.14: Cross beam 71, web 20x900x7420, top flange 25x500x7420, bottom flange 25x600x7420

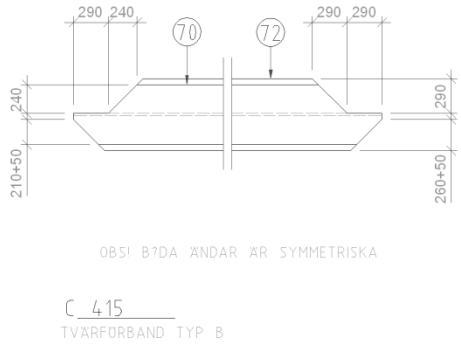

Figure 8.15: C415, Plan view over cross-beam 71 with different widths of the flanges

Main girders

1c and 1d

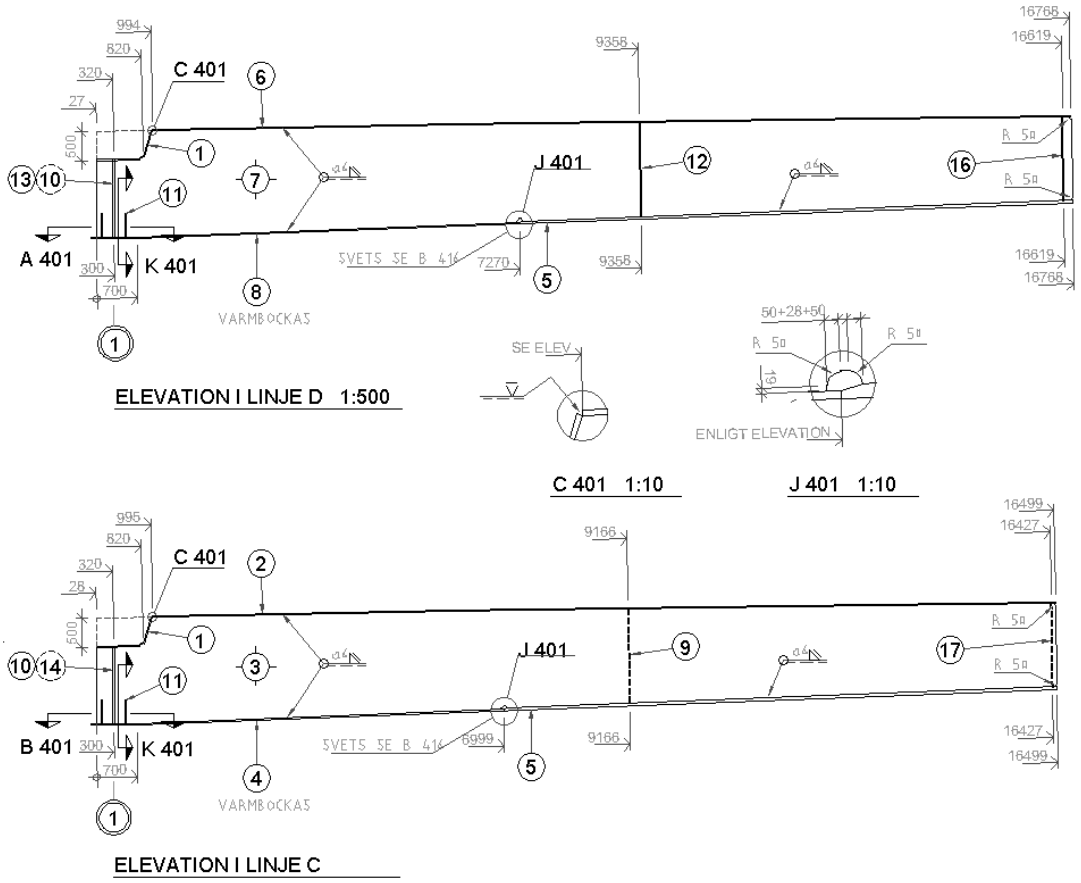

POS	ANT	BENÄMNING	LÄNGD
1	2	™FL PL 20x700	1304
2	1	™FL PL 20x700	15504
3	1	LIV PL 18x1829	16499
4	1	UFL PL 28x900	7101
5	2	UFL PL 47x900	9502
6	1	™FL PL 20x700	15774
7	1	LIV PL 18x1829	16768
8	1	UFL PL 28x900	7372
9	1	PL 20x250	1625
11	8	PL 20x200	400
12	1	PL 20x250	1623
16	1	PL 20x250	1437
17	1	PL 20X250	1435

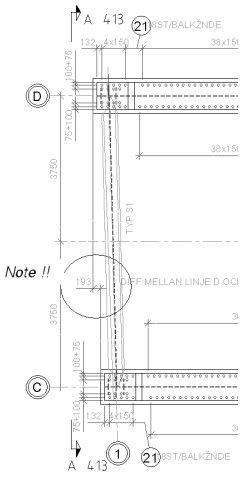

Figure 8.16: The two main girders with dimension at each position. Difference in starting position between the two main girders (193 mm)

Pos 9 and 12 **F1 (**F followed by a number in bold text represents the supports in span)

Pos 16 and 17 **F2**

End support **S1** (S followed by a number in bold text represent the end supports)

2c and 2d

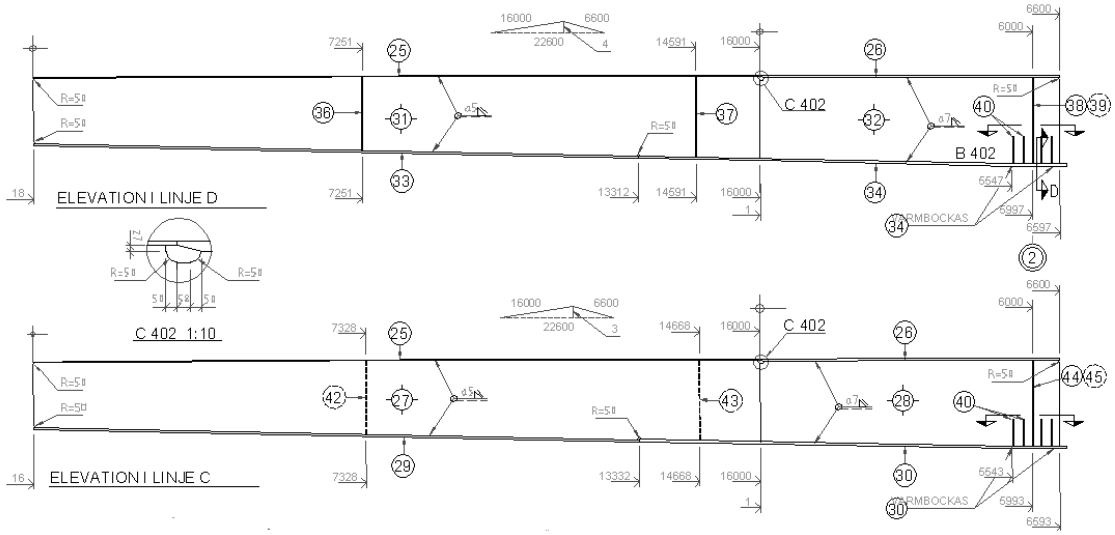

POS	ANT	BENÄMNING	LÄNGD
25	2	TM FL PL 20x700	16000
26	2	TM FL PL 47x700	6600
27	1	LIV PL 18x1817	16000
28	1	LIV PL 20x1907	6600
29	1	UFL PL 47x900	13319
30	1	UFL PL 50x900	9412
31	1	LIV PL 18x1820	16000
32	1	LIV PL 20x1907	6600
33	1	UFL PL 47x900	13297
34	1	UFL PL 50x900	9435
36	1	PL 20x250	1621
37	1	PL 20x250	1775
38	1	PL 25x300	1903
39	1	PL 25x300	1903
40	16	PL 20x300	600
42	1	PL 20x250	1622
43	1	PL 20x250	1776
44	1	PL 25x300	1903
45	1	PL 25x300	1903

Figure 8.17: The two main girders with dimension at each position. Difference between the two main girders (77 mm)

Pos 36 and 42 **F3**

Pos 37 and 43 **F4**

Pos 38,39,44,45 **B2** (B followed by a number in bold text represent the end supports)

3c and 3d

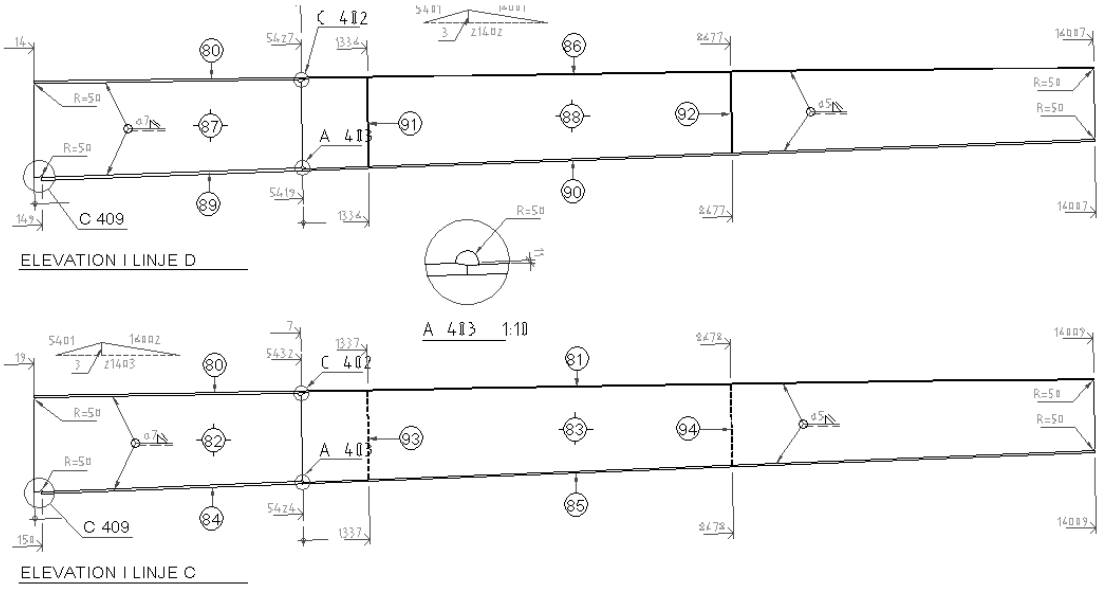

POS	ANT	BENÄMNING	LÄNGD
80	2	TM FL PL 47x700	5413
81	1	TM FL PL 20x700	16002
82	1	LV PL 20x1910	5432
83	1	LV PL 18x1834	16009
84	1	UFL PL 50x900	5281
85	1	UFL PL 39x900	16014
86	1	TM FL PL 20x700	16001
87	1	LV PL 20x1909	5427
88	1	LV PL 18x1834	16007
89	1	UFL PL 50x900	5276
90	1	UFL PL 39x900	16013
91	1	PL 20x250	1790
92	1	PL 20x250	1628
93	1	PL 20x250	1790
94	1	PL 20x250	1628

Figure 8.18: The two main girders with dimension at each position. Difference in starting position between the two main girders (0 mm)

Pos 91 and 93 **F5**

Pos 92 and 94 **F6**

4c and 4d

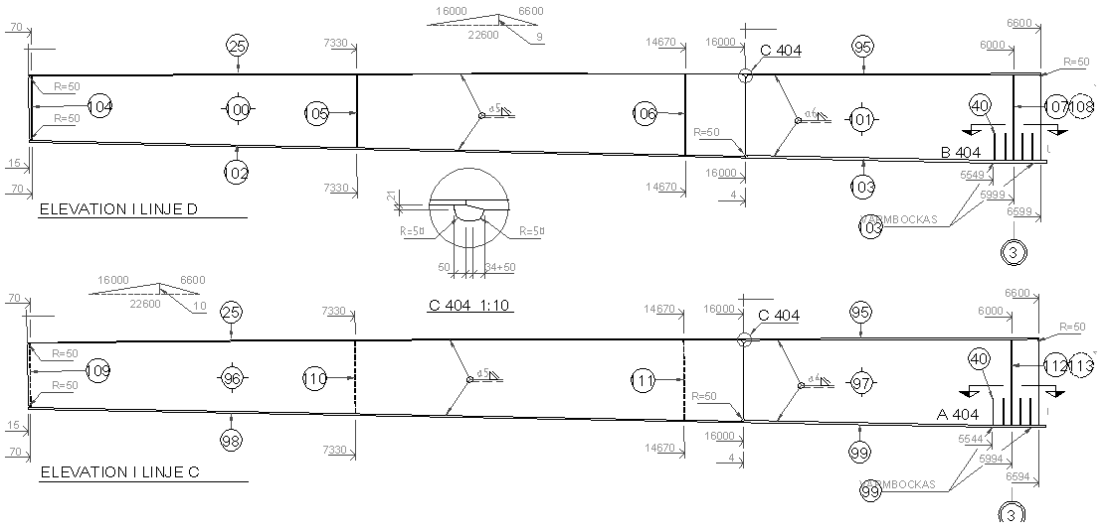

POS	ANT	BENÄMNING	LÄNGD
40	16	PL 20x300	600
25	2	TMFL PL 20x700	16000
95	2	TMFL PL 41x700	6600
96	1	LIV PL 18x1842	16000
97	1	LIV PL 20x1917	6600
98	1	UFL PL 39x900	15989
99	1	UFL PL 45x900	6741
100	1	LIV PL 18x1842	16000
101	1	LIV PL 20x1917	6600
102	1	UFL PL 39x900	15990
103	1	UFL PL 45x900	6745
104	1	PL 20x250	1442
105	1	PL 20x250	1635
106	1	PL 20x250	1719
107	1	PL 25x300	1914
108	1	PL 25x300	1914
109	1	PL 20x250	1442
110	1	PL 20x250	1635
111	1	PL 20x250	1794
112	1	PL 25x300	1914
113	1	PL 25x300	1914

Figure 8.19: The two main girders with dimension at each position

Pos 104 and 109	**F7**
Pos 105 and 110	**F8**
Pos 106 and 111	**F9**
Pos 107, 108, 112, 113	**B3**

5c and 5d

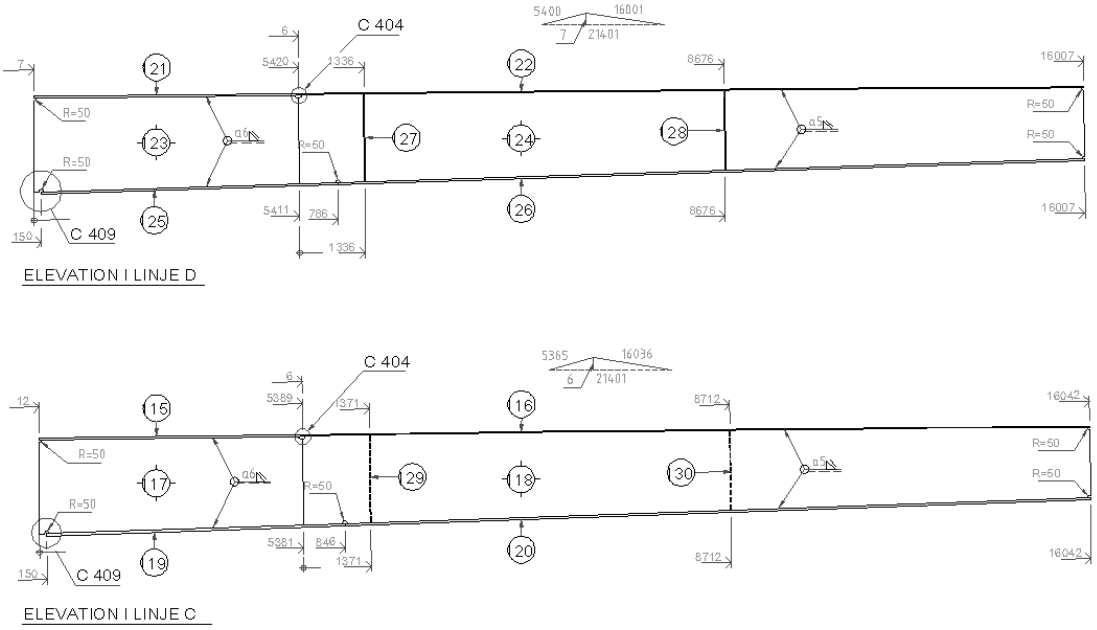

POS	ANT	BENÄMNING	LÄNGD
115	1	TMFL PL 41x700	5377
116	1	TMFL PL 20x700	16036
117	1	LIV PL 20x1920	5389
118	1	LIV PL 18x1830	16042
119	1	UFL PL 45x900	6079
120	1	UFL PL 42x900	15201
121	1	TMFL PL 41x700	5413
122	1	TMFL PL 20x700	16001
123	1	LIV PL 20x1919	5420
124	1	LIV PL 18x1830	16007
125	1	UFL PL 45x900	6049
126	1	UFL PL 42x900	15225
127	1	PL 20x250	1790
128	1	PL 20x250	1627
129	1	PL 20x250	1790
130	1	PL 20x250	1626

Figure 8.20: The two main girders with dimension at each position

Pos 127 and 129 **F10**

Pos 128 and 130 **F11**

6c and 6d

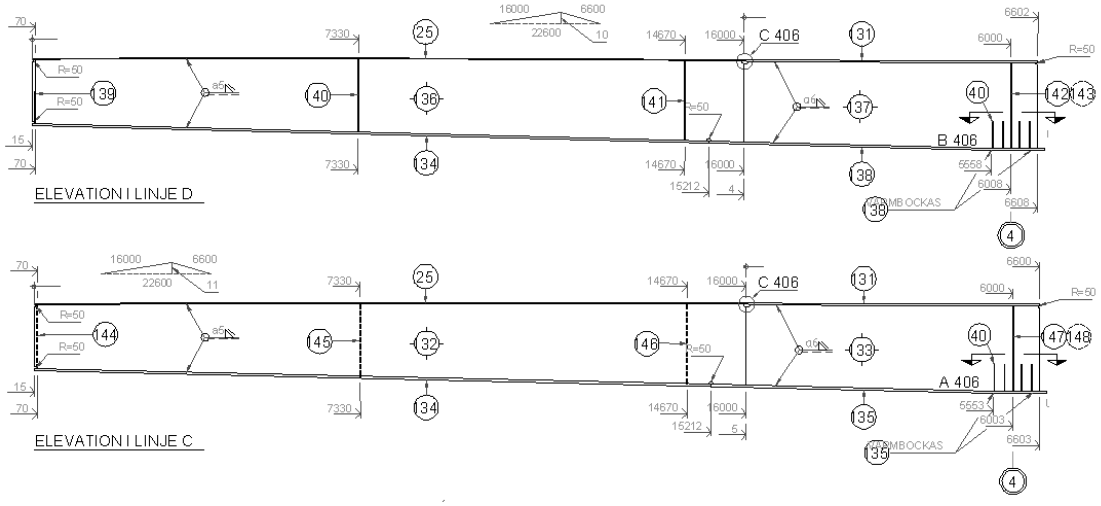

POS	ANT	BENÄMNING	LÄNGD
40	16	PL 20x300	600
25	2	TMFL PL 20x700	16000
131	2	TMFL PL 42x700	6602
132	1	LIV PL 18x1839	16000
133	1	LIV PL 20x1913	6603
134	2	UFL PL 42x900	15201
135	1	UFL PL 47x900	7539
136	1	LIV PL 18x1837	16000
137	1	LIV PL 20x1912	6608
138	1	UFL PL 47x900	7544
139	1	PL 20x250	1439
140	1	PL 20x250	1635
141	1	PL 20x250	1794
142	1	PL 25x300	1911
143	1	PL 25x300	1911
144	1	PL 20x250	1440
145	1	PL 20x250	1635
146	1	PL 20x250	1795
147	1	PL 25x300	1911
148	1	PL 25x300	1911

Figure 8.21: The two main girders with dimension at each position

Pos 139 and 144	**F12**
Pos 140 and 145	**F13**
Pos 141 and 146	**F14**
Pos 142, 143, 147, 148	**B4**

7c and 7d

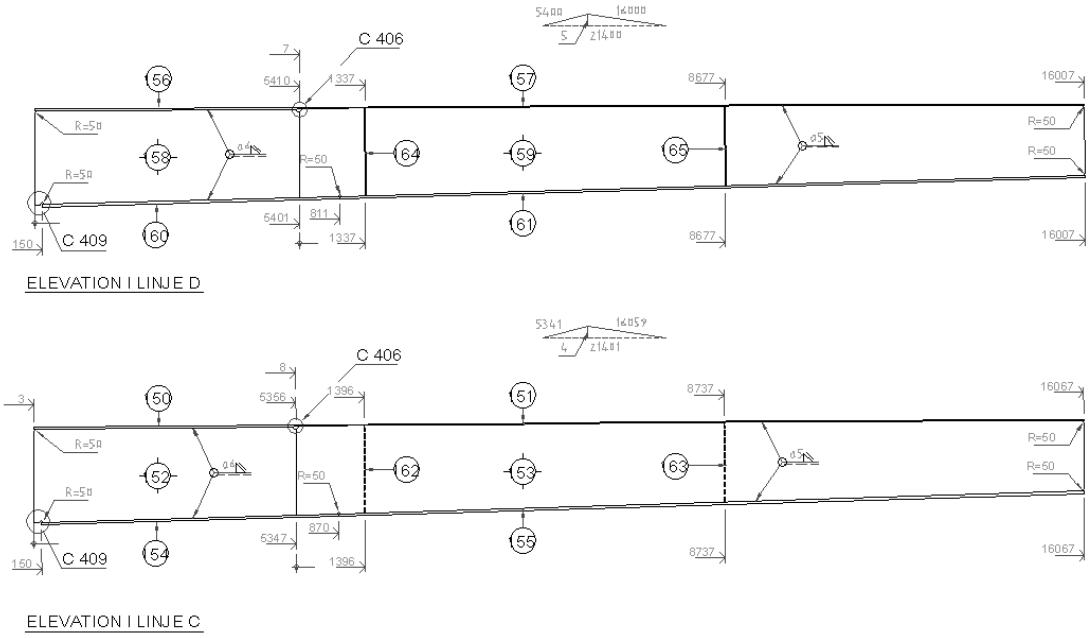

POS	ANT	BENÄMNING	LÄN
150	1	™FL PL 42x700	5353
151	1	™FL PL 20x700	16059
152	1	LIV PL 20x1915	5356
153	1	LIV PL 18x1825	16067
154	1	UFL PL 47x900	6069
155	1	UFL PL 42x900	15201
156	1	™FL PL 42x700	5410
157	1	™FL PL 20x700	16000
158	1	LIV PL 20x1914	5410
159	1	LIV PL 18x1824	16007
160	1	UFL PL 47x900	6065
161	1	UFL PL 42x900	15200
162	1	PL 20x250	1786
163	1	PL 20x250	1624
164	1	PL 20x250	1786
165	1	PL 20x250	1625

Figure 8.22: The two main girders with dimension at each position

Pos 162 and 164 **F15**

Pos 163 and 165 **F16**

8c and 8d

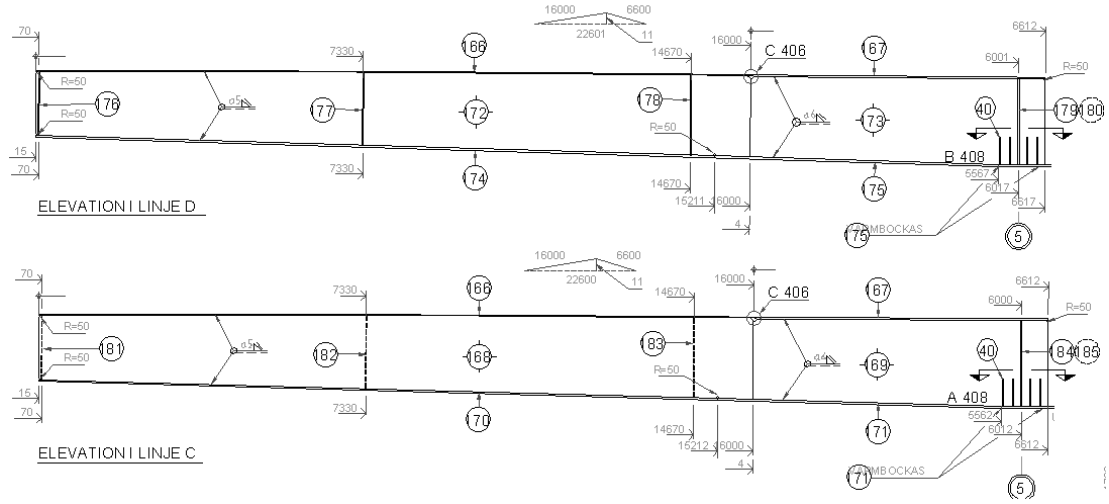

POS	ANT	BENŽMNING	LŽNGD
40	16	PL 20x300	600
166	2	™FL PL 20x700	16000
167	2	™FL PL 42x700	6612
168	1	LIV PL 18x1842	16000
169	1	LIV PL 20x1916	6612
170	1	UFL PL 42x900	15201
171	1	UFL PL 47x900	7548
172	1	LIV PL 18x1843	16000
173	1	LIV PL 20x1917	6617
174	1	UFL PL 42x900	15199
175	1	UFL PL 47x900	7555
176	1	PL 20x250	1439
177	1	PL 20x250	1638
178	1	PL 20x250	1796
179	1	PL 25x300	1911
180	1	PL 25x300	1911
181	1	PL 20x250	1440
182	1	PL 20x250	1638
183	1	PL 20x250	1796
184	1	PL 25x300	1911
185	1	PL 25x300	1911

Figure 8.23: The two main girders with dimension at each position

Pos 176 and 181	**F17**
Pos 177 and 182	**F18**
Pos 178 and 183	**F19**
Pos 179, 180, 184, 185	**B5**

9c and 9d

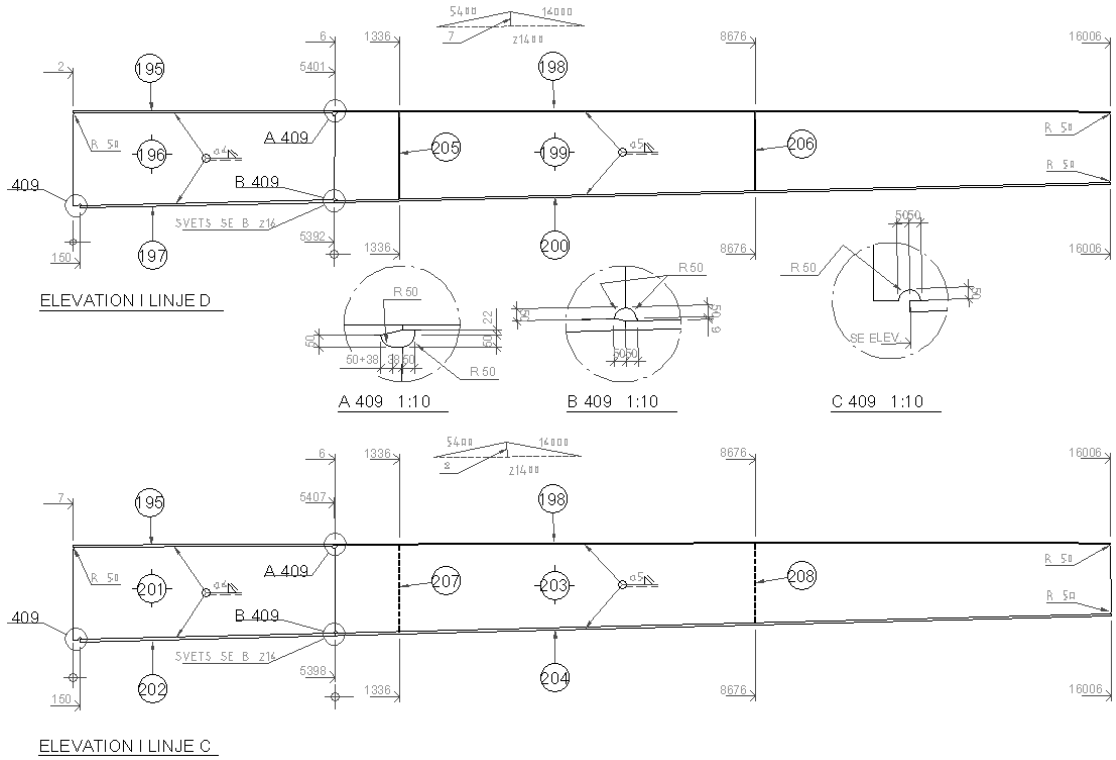

POS	ANT	BENŽMNING	LŽNGD
195	2	™FL PL 42x700	5400
196	1	LIV PL 20x1911	5401
197	1	UFL PL 47x900	5244
198	2	™FL PL 20x700	16000
199	1	LIV PL 18x1835	16006
200	1	UFL PL 38x900	16011
201	1	LIV PL 20x1912	5407
202	1	UFL PL 47x900	5249
203	1	LIV PL 18x1837	16006
204	1	UFL PL 38x900	16010
205	1	PL 20x250	1792
206	1	PL 20x250	1631
207	1	PL 20x250	1794
208	1	PL 20x250	1631

Figure 8.24: The two main girders with dimension at each position

Pos 205 and 207 **F20**

Pos 206 and 208 **F21**

10c and 10d

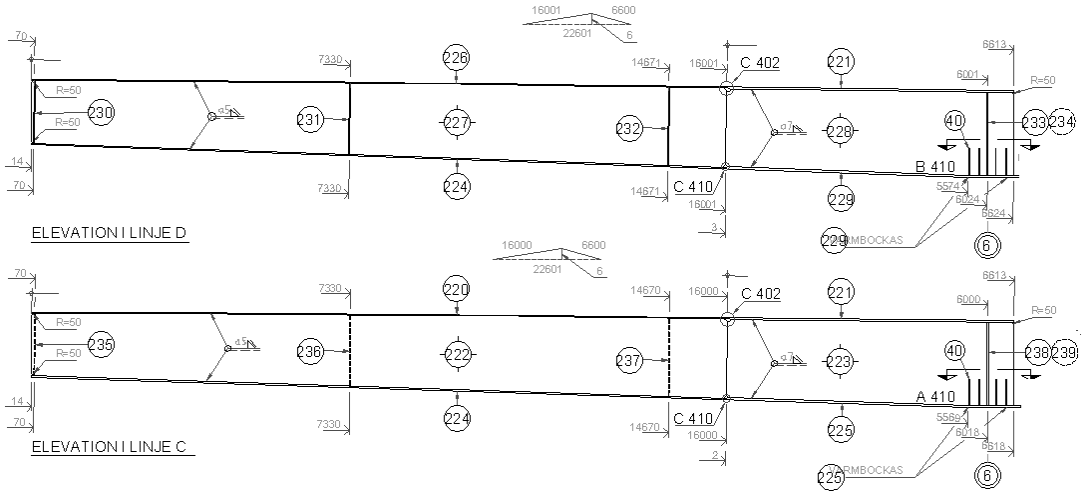

POS	ANT	BENÄMNING	LÄNGD
40	16	PL 20x300	600
220	1	™FL PL 20x700	16000
221	2	™FL PL 47x700	6613
222	1	LIV PL 18x1841	16000
223	1	LIV PL 20x1910	6618
224	2	UFL PL 38x900	15991
225	1	UFL PL 50x900	6768
226	1	™FL PL 20x700	16001
227	1	LIV PL 18x1842	16001
228	1	LIV PL 20x1911	6624
229	1	UFL PL 50x900	6773
230	1	PL 20x250	1444
231	1	PL 20x250	1635
232	1	PL 20x250	1796
233	1	PL 25x300	1903
234	1	PL 25x300	1903
235	1	PL 20x250	1444
236	1	PL 20x250	1634
237	1	PL 20x250	1794
238	1	PL 25x300	1903
239	1	PL 25x300	1903

Figure 8.25: The two main girders with dimension at each position

Pos 230 and 235	**F22**
Pos 231 and 236	**F23**
Pos 232 and 237	**F24**
Pos 233, 234, 238, 239	**B6**

11c and 11d

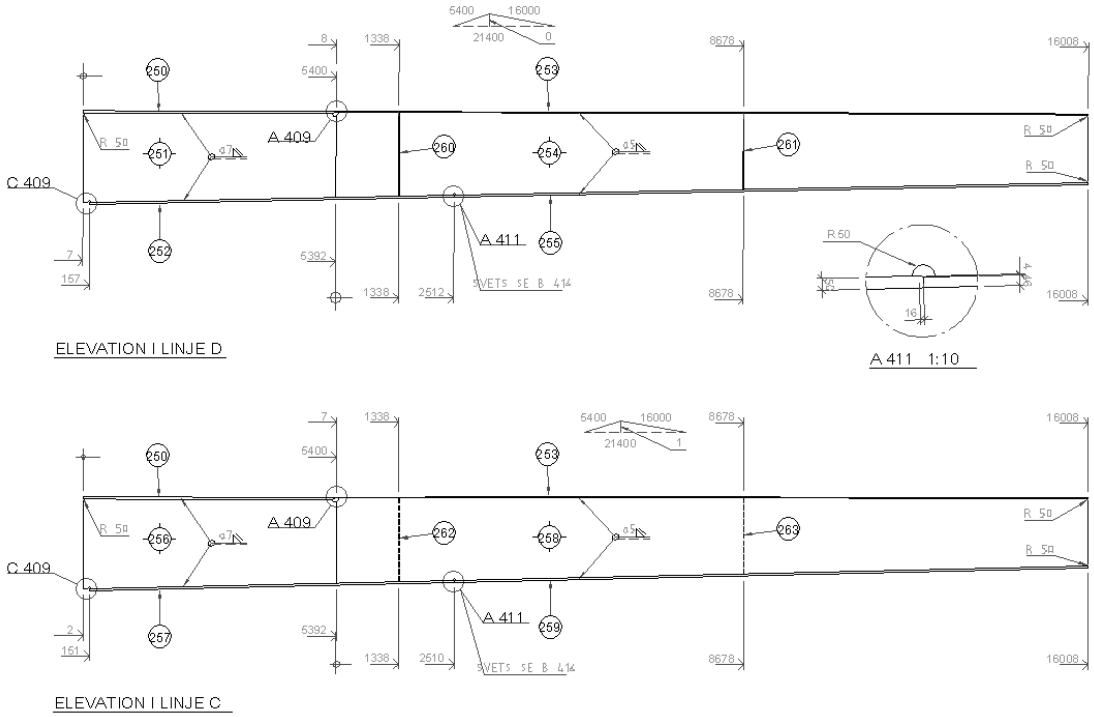

POS	ANT	BENŽMNING	LŽNGD
250	2	™FL PL 47x700	5400
251	1	LIV PL 20x1897	5400
252	1	UFL PL 50x900	7750
253	2	™FL PL 20x700	16000
254	1	LIV PL 18x1812	16008
255	1	UFL PL 46x900	13500
256	1	LIV PL 20x1898	5400
257	1	UFL PL 50x900	7754
258	1	LIV PL 18x1814	16008
259	1	UFL PL 46x900	13501
260	1	PL 20x250	1771
261	1	PL 20x250	1615
262	1	PL 20x250	1773
263	1	PL 20x250	1615

Figure 8.26: The two main girders with dimension at each position

Pos 260 and 262 **F25**

Pos 261 and 263 **F26**

12c and 12d

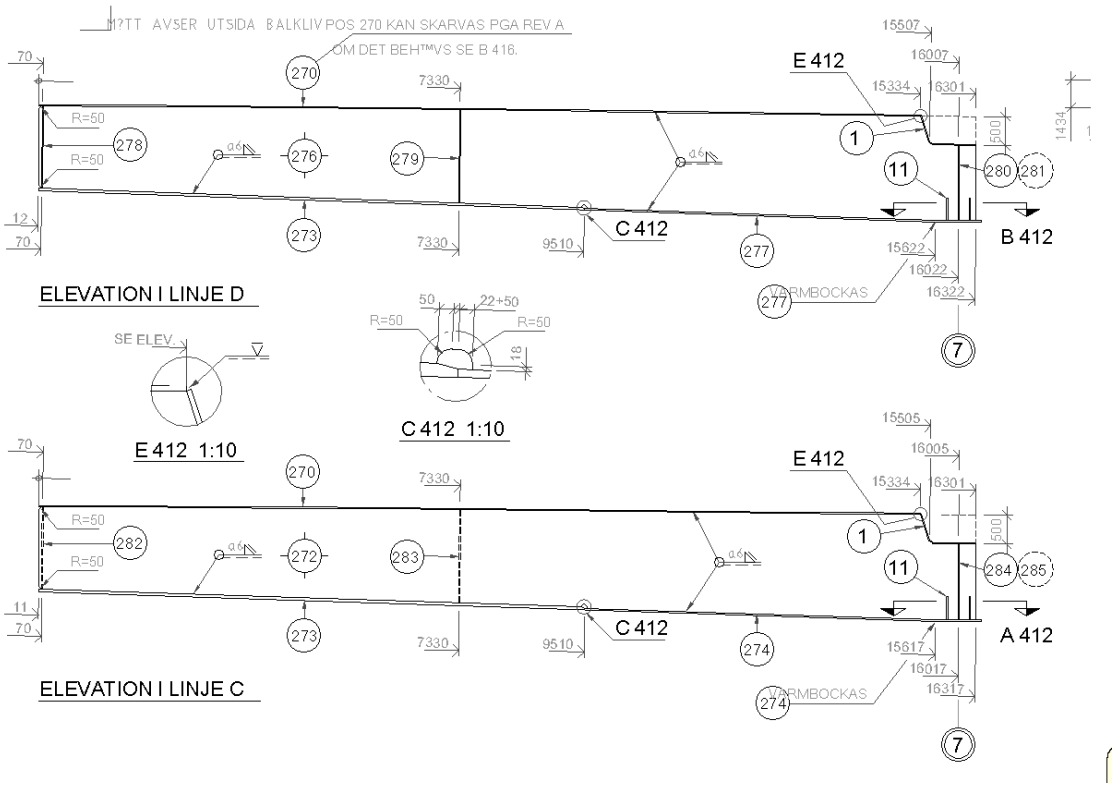

POS	ANT	BENŽMNING	LŽNGD
1	2	PL 20x700	1304 2134
11	8	PL 20x200	400 2134
21	194	STUDS í 22 ENL BN 88 KAP 54.31	
22	196	STUDS í 22 ENL BN 88 KAP 54.31	
270	2	™FL PL 20x700	15334
271	1	™FL PL 20x700	1700
272	1	LIV PL 18x1834	16317
273	2	UFL PL 46x900	9501
274	1	UFL PL 28x900	6910
275	1	™FL PL 20x700	1701
276	1	LIV PL 18x1835	16322
277	1	UFL PL 28x900	6915
278	1	PL 20x250	1436
279	1	PL 20x250	1622
280	1	PL 25x250	1314
281	1	PL 25x250	1314
282	1	PL 20x250	1436
283	1	PL 20x250	1622
284	1	PL 25x250	1314
285	1	PL 25x250	1314

Figure 8.27: The two main girders with dimension at each position

Pos 278 and 282 **F27**

Pos 279 and 283 **F28**

End support **S7**

Appendix B: Hand calculations of small-scale model

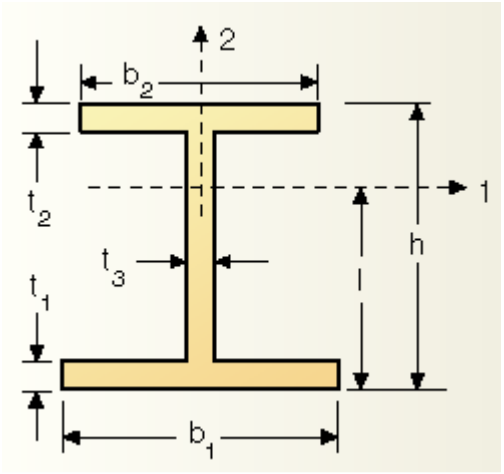

$b_1 := 250\,mm$

$b_2 := 250\,mm$

$t_1 := 20\,mm$

$t_2 := 20\,mm$

$t_3 := 15\,mm$

$b_{deck} := 300\,mm$

$t_{deck} := 250\,mm$

$z_{f1} := 10\,mm$

$z_{f2} := 690\,mm$

$z_{NA} := \frac{700}{2}\,mm$

$z_w := 350\,mm$

$h_w := 660\,mm$

$L := 4m$

$q_d := 1MPa \cdot b_1 = 250 \frac{kN}{m}$ $\quad P := 1kN$ $\quad E := 200GPa$ $\quad \alpha_1 := \frac{34}{210}$

$$z_{na} := \frac{b_{deck} \cdot t_{deck} \cdot \frac{t_{deck}}{2} \cdot \alpha_1 + b_1 \cdot t_1 \cdot \left(t_{deck} + \frac{t_1}{2} \right) \ldots + h_w \cdot t_3 \cdot \left(t_{deck} + t_1 + \frac{h_w}{2} \right) + b_2 \cdot t_2 \cdot \left(t_1 + t_{deck} + h_w + \frac{t_2}{2} \right)}{b_{deck} \cdot t_{deck} \cdot \alpha_1 + b_1 \cdot t_1 + h_w \cdot t_3 + b_2 \cdot t_2} = 0.42m$$

$$I_y := \frac{b_{deck} \cdot t_{deck}^3}{12} \cdot \alpha_1 + b_{deck} \cdot t_{deck} \cdot \alpha_1 \cdot \left(\frac{t_{deck}}{2} - z_{na} \right)^2 \ldots = 3.28 \times 10^{-3}\, m^4$$
$$+ \frac{b_1 \cdot t_1^3}{12} + b_1 \cdot t_1 \cdot \left(t_{deck} + \frac{t_1}{2} - z_{na} \right)^2 \ldots$$
$$+ \frac{t_3 \cdot h_w^3}{12} + t_3 \cdot h_w \cdot \left(t_{deck} + t_1 + \frac{h_w}{2} - z_{na} \right)^2 \ldots$$
$$+ \frac{b_2 \cdot t_2^3}{12} + b_2 \cdot t_2 \cdot \left(t_{deck} + t_1 + h_w + \frac{t_2}{2} - z_{na} \right)^2$$

$\delta_{hand} := \frac{5 \cdot q_d \cdot L^4}{384 \cdot E \cdot I_y} = 1.27 \times 10^{-3}\, m$ $\quad \delta_{ABAQUS} := 1.215 \cdot 10^{-3}\, m$ $\quad \frac{\delta_{ABAQUS}}{\delta_{hand}} \cdot 100 = 95.658$

Appendix C: Mesh evaluation

Table 8.1: Element sizes in the mesh evaluation; The table show deviation from the size 200 mm in percent

		[%]						
Check point		Size mm	1750	1500	1250	1000	750	600
1	S1.1	Load 1	0.85751	0.58014	0.5874	0.33908	-0.1975	-0.7101
		Load 2	-0.0684	-0.3612	-0.3488	-0.6033	-1.1636	-1.6659
		Load 3	-2.3271	-2.6449	-2.6087	-2.8768	-3.4602	-3.9219
2	S1.1	Load 1	2.11443	2.2811	2.42607	2.56365	2.90241	3.13417
		Load 2	9.09014	9.10561	9.08085	9.05146	8.85809	8.70958
		Load 3	21.8394	21.4912	21.1081	20.7509	19.5605	18.6854
1	U2	Load 1	0.10245	0.10245	0.09944	0.10305	0.10607	0.10667
		Load 2	-0.9053	-0.9111	-0.9166	-0.9168	-0.9216	-0.9123
		Load 3	-2.8064	-2.8255	-2.8358	-2.8468	-2.8696	-2.8445
			500	400	300	250	220	200
1	S1.1	Load 1	0.35796	-0.5424	0.57869	-0.077	-0.3805	_
		Load 2	-0.4049	-1.0513	0.13611	-0.4244	-0.6446	_
		Load 3	-2.1913	-2.2384	-0.8936	-1.2295	-1.2511	_
2	S1.1	Load 1	2.87825	3.09225	1.39647	1.80525	1.62675	_
		Load 2	7.03418	6.75959	2.55486	2.3816	1.61661	_
		Load 3	14.6342	13.4664	4.71016	3.5144	1.69129	_
1	U2	Load 1	0.07774	0.04882	0.03556	0.02531	0.01205	_
		Load 2	-0.7802	-0.4538	-0.3964	-0.2883	-0.168	_
		Load 3	-2.4105	-1.4067	-1.2169	-0.8837	-0.5093	_

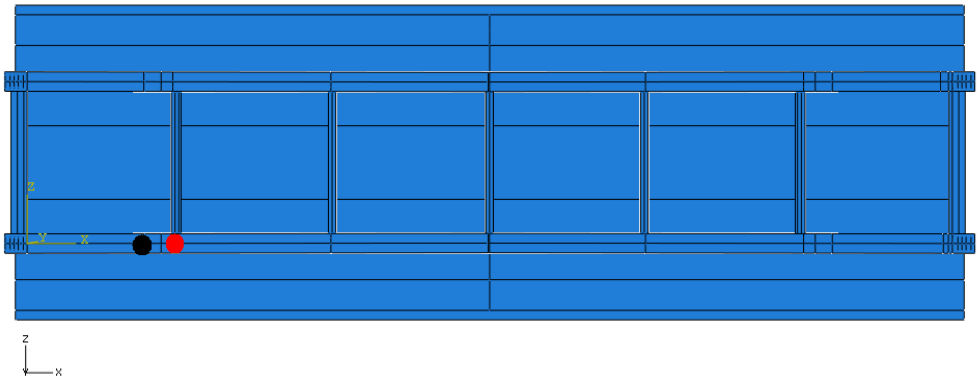

Figure 8.28: The black dot representing checkpoint 1 and the red checkpoint 2

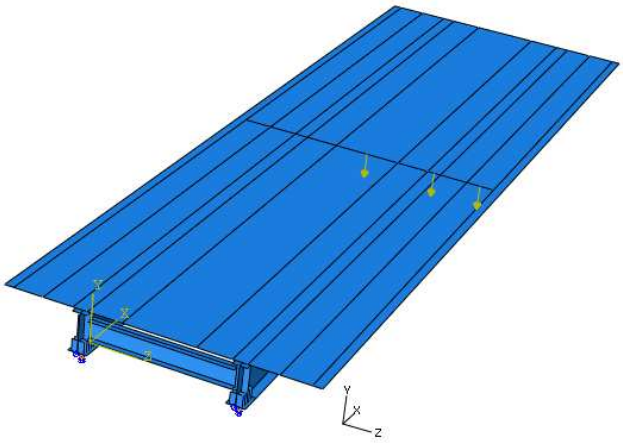

Figure 8.29: Applied load; Load 1 in centre, load 2 over top flange and load 3 at console

Appendix D: Additional diagrams from verification

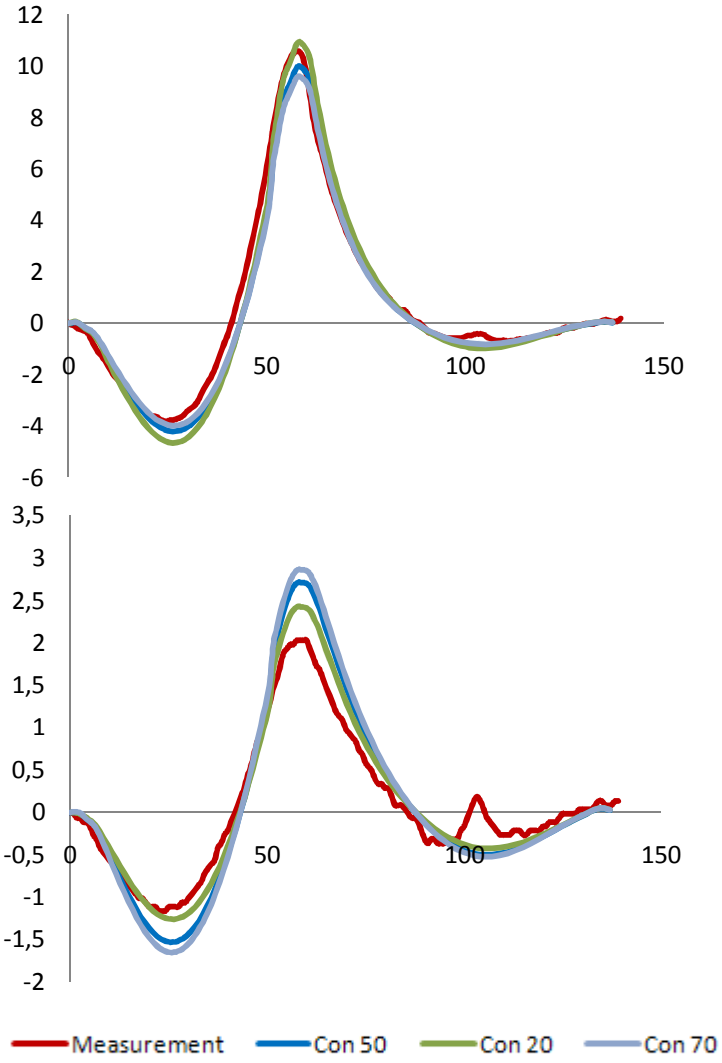

Figure 8.30: Different concrete stiffness, Ch 8 and 4, right lane

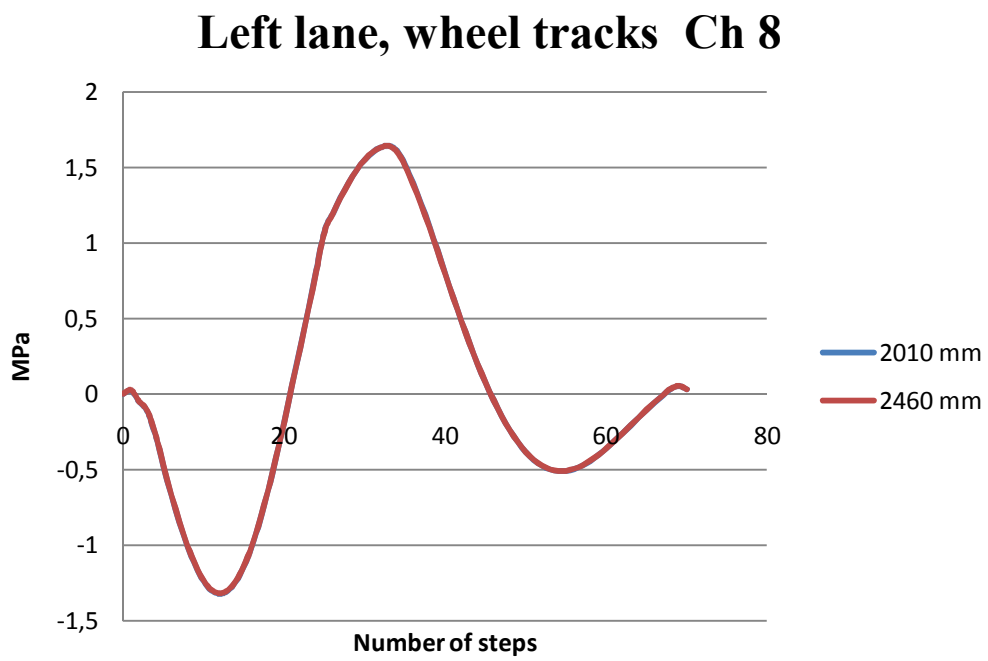

Figure 8.31: Different wheel tracks distances of the moving load

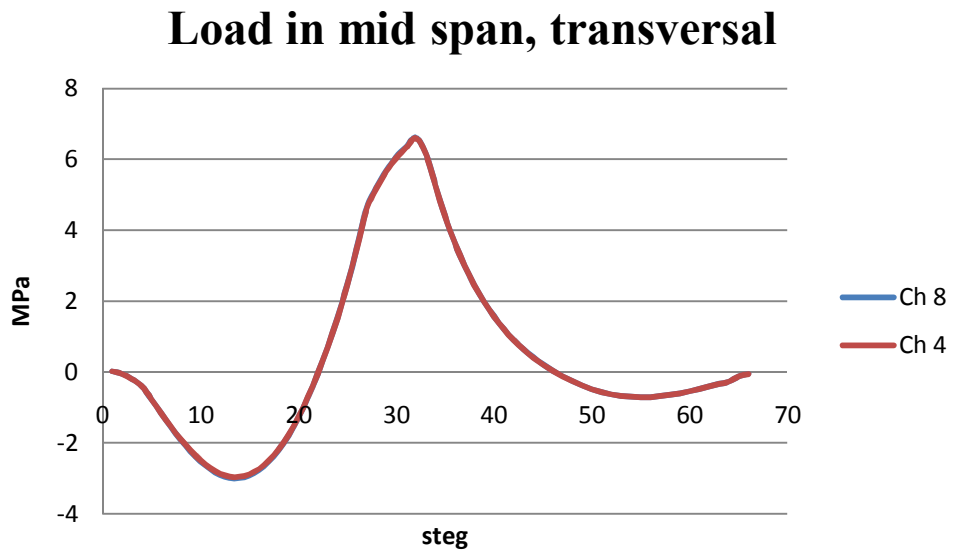

Figure 8.32: Load in mid span, symmetry check of the bridge model

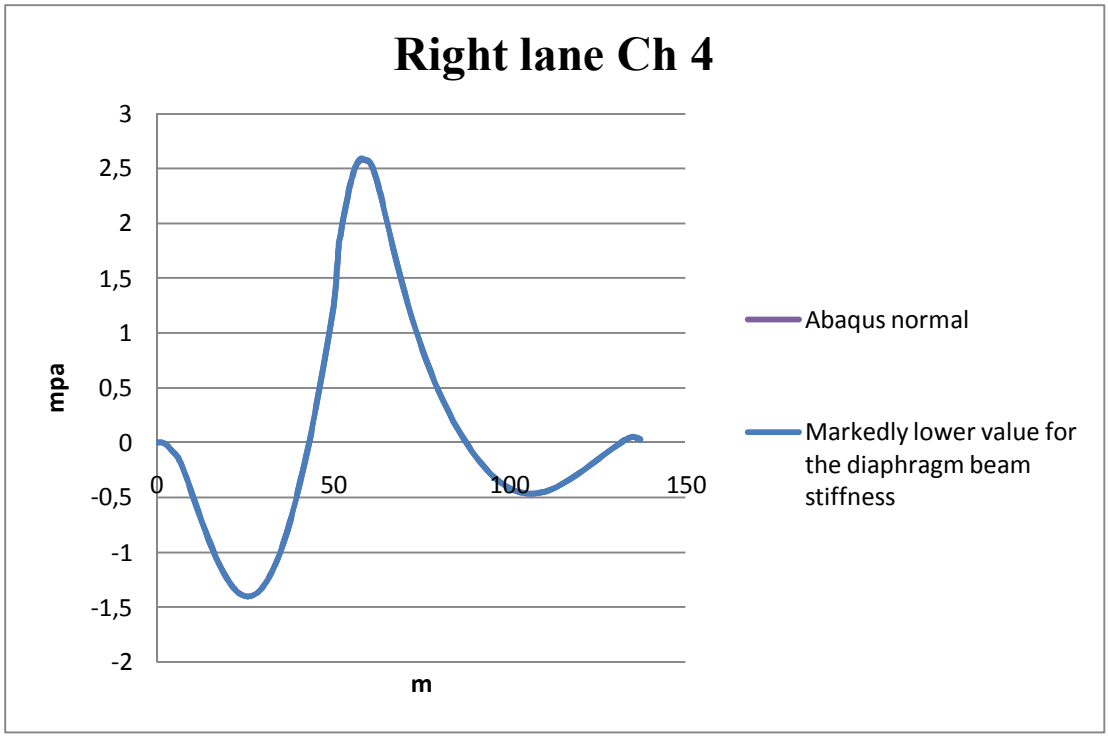

Figure 8.33: Lower stiffness of the diaphragm beam compared the normal value